UNIVERSITY of CALIFORNIA
SANTA CRUZ

STRUCTURAL EVOLUTION OF STAR-FORMING GALAXIES FROM COSMOLOGICAL SIMULATION AT $1 < z < 3$

A thesis submitted in partial satisfaction of the
requirements for the degree of

BACHELOR OF SCIENCE

in

ASTROPHYSICS

by

Vivian L. Tang

June 11, 2015

The thesis of Vivian L. Tang is approved by:

Professor Joel R Primack
Advisor

Professor Adriane Steinacker
Theses Coordinator

Professor Robert P Johnson
Chair, Department of Physics

Abstract

Structural Evolution of Star-forming Galaxies from Cosmological Simulation at $1 < z < 3$

by

Vivian L. Tang

Recent Hubble Space Telescope (HST) observations of galaxies in the Cosmic Assembly Near-infrared DEEP Extragalactic Legacy Survey (CANDELS) indicate that a majority of star-forming galaxies with stellar masses less than about $10^{9.5} M_{\odot}$ are elongated at $1.5 < z < 2$, while for galaxies of similar stellar masses in the local Universe, the most common structures are disks and spheroids. In this thesis we analyze images of star-forming galaxies from hight-resolution, zoom-in cosmological simulations and systematically compare our findings to those from HST observations. These images were obtained using the Sunrise code, which takes into account stellar evolution and the effects of dust. Their resolution is reduced and noise is added for proper comparison with CANDELS galaxy images, a process called CANDELization. Measurements of the structural parameters effective radius, Sérsic index, and projected axis ratios of our simulated galaxy images are obtained using the data analysis algorithm GALFIT, a program also used for the analysis on CANDELS galaxy images. Image fitting via GALFIT is accomplished by a single-component fit with the Sérsic function. Our sample consists of five pairs of galaxies simulated using the Adaptive Mesh Refinement (ART) code and are studied in edge-on, face-on, and random viewing angles. There are two types of simulations: with and without radiative pressure (RP) feedback. Galaxies generated with RP feedback more closely resemble the observed star-forming galaxies from CANDELS in terms of star formation rate (SFR) and stellar mass, giving rise to structure and morphology that are different than galaxies generated without RP feedback.

The stellar masses for our sample galaxies are $10^{9.2} - 10^{10} M_{\odot}$ at $z \sim 2$ and $10^{9.6} - 10^{10.3} M_{\odot}$ at $z \sim 1$. A recent paper analyzing the axis ratio distributions of star-forming galaxies

from CANDELS found that a majority of galaxies with stellar masses $10^9 - 10^{9.5} M_\odot$ at $1 < z < 2.5$ and stellar masses $10^{9.5} - 10^{10} M_\odot$ at $1.5 < z < 2.5$ are elongated (i.e., prolate, with one long and two short axes). At $z < 1$ most star-forming galaxies have disk-like structure, and the projected axis ratio distributions peak at a value of ~ 0.3 for galaxies with stellar masses $10^9 - 10^{10} M_\odot$ at $1.5 < z < 2$, suggesting elongation.

We find that four out of five simulations with RP feedback have similar structures at different redshifts: VELA02MRP are elongated at $z \sim 2$, VELA05MRP and VELA27MRP are elongated at $1.5 < z < 2$, and galaxies from VELA28MRP are likely to be elongated at $z \sim 1.5$ from the analysis on their structural parameters, while from inspecting their images in both high-resolution and H band we find that they look elongated at $1.5 < z < 2$. The results of our five simulations without RP feedback are less conclusive due to too few data points. However, it is clear that the two types of galaxies evolve differently due to RP feedback. The shapes inferred from face-on and edge-on analysis generally do not agree with results from random viewing angles. Upon inspection, we find that the random angles were not truly random, and the sky background parameter in GALFIT was not defined properly; furthermore, from inspecting both the high resolution and CANDELized images, we find that certain images contain more than one object (satellite or minor merger) which causes GALFIT to fit our data improperly. We find that data with acceptable uncertainties are reliable while the results from random angles need to be reconsidered. We suspect that all inconclusive results from this study will be more conclusive when better defined parameters are provided to GALFIT during the continuation of this research in summer 2015.

To the stars,

without names,

I adore you.

Contents

1 Introduction

1.1 Observations

The shapes of galaxies is a fascinating subject in the field of Astrophysics. Much effort has been devoted to both theoretical work with computer simulations and observational work with advancements in ground and space based telescopes. While some observers are interested in detections of faint, high redshift galaxies, others are analyzing galaxies in the local Universe in great detail. Together insights into the physics responsible for their evolution have been gained through the study of their shapes. From both theory and observation, it is estimated that formation of the first galaxies (dwarf galaxies) began as early as when the Universe was 100 Myr old. As the first stars began to form out of the cold dense primordial gas clouds near the end of the cosmic dark ages, emitted radiation ionized HI in their surroundings. Giving rise to the first galaxies, some of these young stars eventually went supernova creating heavy elements which seeded the formation of the next generation low metallicity stars (Population II), and eventually evolved to the present-day (Population I) stars (Loeb, 2010). In the ΛCDM model cosmology, the size of galaxies grew hierarchically. Starting from initial density perturbations, formation of dark matter halos, cooling of gas, to formation of young stars and dwarf galaxies, small objects formed first: merging of small galaxies in the past gave rise to the sizes of present-day galaxies that are much bigger. It also resulted in dramatic changes in their geometries, stellar distributions, and generated high SFRs responsible for morphological transformation (O'Leary and Kartaltepe, 2013). It has been shown that at early epochs, stars formed over a shorter time period in more massive galaxies (archaeological downsizing) and that star-forming galaxies at higher redshifts are more massive than those at low redshift (downsizing in time) (Neistein et al., 2006). For similar stellar mass, high redshift galaxies have higher SFR than those of the present-day (Wuyts et al., 2011). It is clear that galaxies underwent major transformations as the stellar population evolved, which have been observed in the Universe as well as in computer simulations.

Observationally speaking, we are limited to obtain only snapshots of galaxy evolution histories at certain stages. Theorists, on the other hand, can study the physics responsible for the formation and evolution of galaxies over a wide range of redshifts in a continuous fashion through cosmological simulations, something that is impossible to witness on the human time scale. For this work, we study star-forming galaxies' structural and morphological evolution at $1 < z < 3$ generated from cosmological simulation and compare results

with galaxies observed by the Hubble Space Telescope (HST) as part of the Cosmic Assembly Near-infrared Deep Extragalactic Legacy Survey (CANDELS). The Wide Field Camera 3 (WFC3) on the HST has both UV/visible and IR detectors, and observations made in the near-infrared waveband (H band) with the IR detector allow observers to study the full stellar population to $z \sim 2$, and young stellar population out to $z \sim 7$. Although our simulated galaxies are generated in many wavebands, for this study we analyze their appearances in H band at $1 < z < 3$. These redshifts mark a crucial period as major morphological transformation has been observed, where star formation rate (SFR) was the highest ($1.5 < z < 6$), an epoch known as the 'cosmic high noon'. By systematic comparison between findings from the CANDELS and star-forming galaxies from our cosmological simulations, we hope to gain insight into the geometrical dependence on stellar mass, size, and redshifts. We do this by analyzing the surface brightness distribution of our simulated galaxies via structural parameters effective radius R_{eff} and Sérsic index n in a way comparable to the analysis previously performed on CANDELS galaxies. Moreover, together with the structural parameters, we exploit the axis ratio of our star-forming galaxies to infer their 3-D geometries and compare to previous findings on the reconstructed 3-D geometry of CANDELS galaxies.

During the epoch of 'cosmic high noon' galaxies were forming stars rapidly, and the highest spectroscopically confirmed redshift galaxy 'z8_GND_5296' measured to have a redshift of 7.5 (Finkelstein et al., 2013) also measured to have a SFR 150 times higher in comparison with our galaxy the Milky Way. The galaxy main sequence, a tight correlation between SFR and stellar mass has been observed through the study of these galaxies. Analysis on the dependence of Sérsic index and size of galaxies from HST at $0.5 < z < 1.5$ and $1.5 < z < 2.5$ (Wuyts et al., 2011) has shown that star-forming galaxies on the main sequence across all redshifts approximated as exponential disk (Sérsic $n \sim 1$). It has also been shown that most low-mass star-forming galaxies at $z < 2$ have exponential surface brightness profiles, and that at $1.5 < z < 2$ galaxies of stellar masses between $\sim 10^9 M_\odot$ to $10^{10} M_\odot$ have median Sérsic index n between 1.0 to 2.0. This is interesting as the distinction between disks and elongated galaxies are not clearly indicated by the Sérsic values, for which the disk and elongated galaxies identified by CANDELS at the same stellar masses and redshifts are not reflected in these Sérsic values.

Another approach to geometrical studies is to reconstruct the 3-D intrinsic shapes of galaxies using correlations between redshift and size. In a previous study (van der Wel et al., 2014) on galaxies at $z < 0.1$ and $1.5 < z < 2.0$ from SDSS, 3D-HST AND CANDELS, the 3-D intrinsic shapes of galaxies were reconstructed based on the observed 2-D geometry.

The 2-D geometries are described as the axis ratio which measures the amount of flattening from the short axis to the long axis. By assuming a triaxial ellipsoid geometry as the 3-D shape, a best-fitting model can be found by projecting the triaxial ellipsoid at random angles to obtain the projected axis ratio distribution, and compare their probability density profile to that of the observed axis ratio distributions. The geometric form of the ellipsoid used in obtaining the best-fitting models for a triaxial ellipsoid population has three axis lengths $A \geq B \geq C$, where the ellipticity and triaxiality is given by $1 - C$ and $(1 - B^2)/(1 - C^2)$, respectively, with $A = 1$. There are three types of 3-D shapes defined from these axis lengths: $A \sim B > C$ is disk-like (oblate), $A > B \sim C$ is elongated (prolate); $A \sim B \sim C$ is round. Figure 1 below shows the colour assigned to each of the shapes.

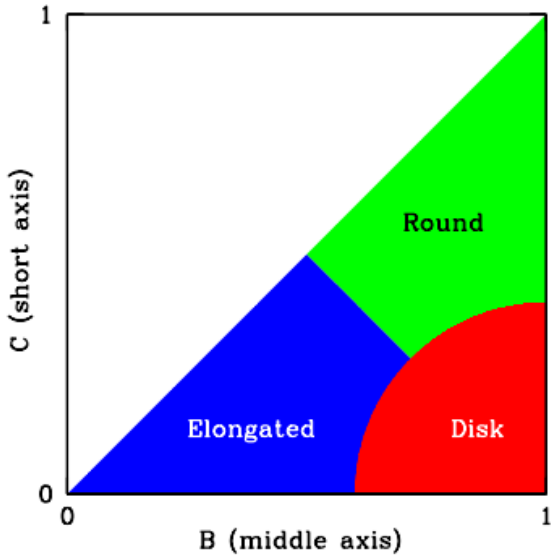

Figure 1: Definition of 3-D shapes. Green is round (three long axes), red is disk-like (two long and one short axis), and blue is elongated (one long and two short axes) (van der Wel et al., 2014).

Using the projected axis ratio distribution from the model population described above and taking into account the effect of random uncertainties of measurements, the observed axis ratio distribution fits well with the probability distributions of triaxial populations of objects seen at random viewing angles as shown in Figure 2. The continuous lines correspond to the best-fitting models and the histograms are the observed distributions. The projected axis ratio distributions peak at a value of ~ 0.3 for galaxies with stellar masses $10^9 - 10^{10} M_\odot$ at $1.5 < z < 2$. And as seen in higher stellar masses, a more evenly distributed axis ratios indicate most galaxies are disk-like, whereas a peak towards large values corresponds to spherical objects.

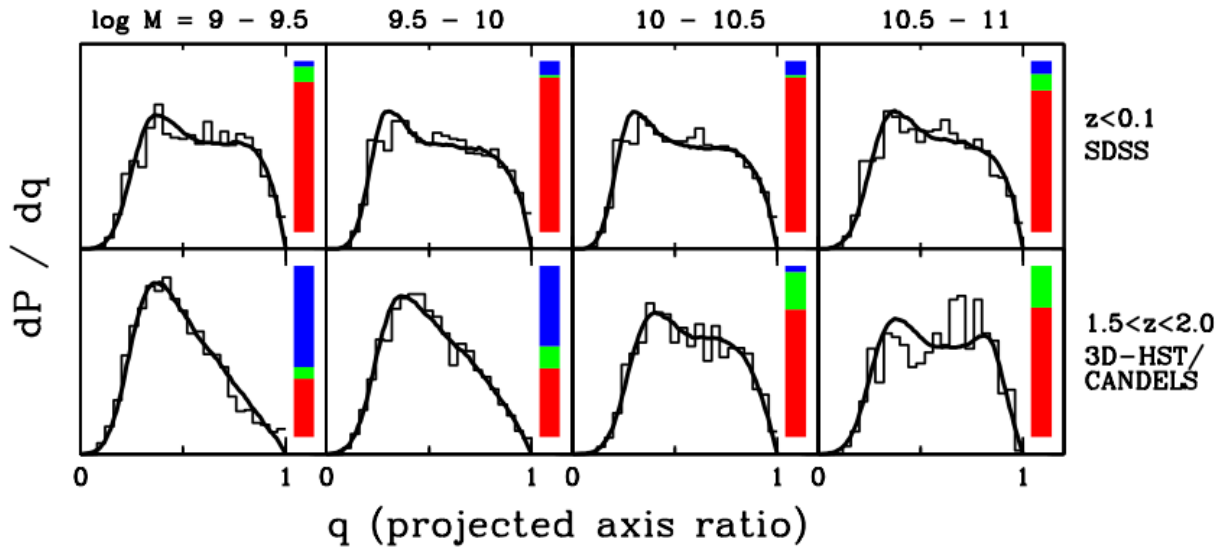

Figure 2: Projected axis ratio distributions as a function of redshift and stellar mass for both the best-fitting model (in continuous lines) and observed data (histograms) (van der Wel et al., 2014).

In terms of stellar mass, a high fraction of galaxies in the lower-mass range with stellar masses of $10^9 - 10^{9.5} M_\odot$ at $1 < z < 2.5$ and $10^{9.5} - 10^{10} M_\odot$ at at $1.5 < z < 2.5$ were found to be elongated, rather than disk-like or spherical. The majority of the present-day star forming galaxies in a wide rage of masses were found to be thin, nearly oblate. And at $z \lesssim 2$ most galaxies with masses greater than $10^{10} M_\odot$ are disk-like. Figure 3 shows this finding: the fraction of galaxies with a certain 3-D geometry (indicated by colour bars) is shown as a function of redshift in four stellar mass intervals.

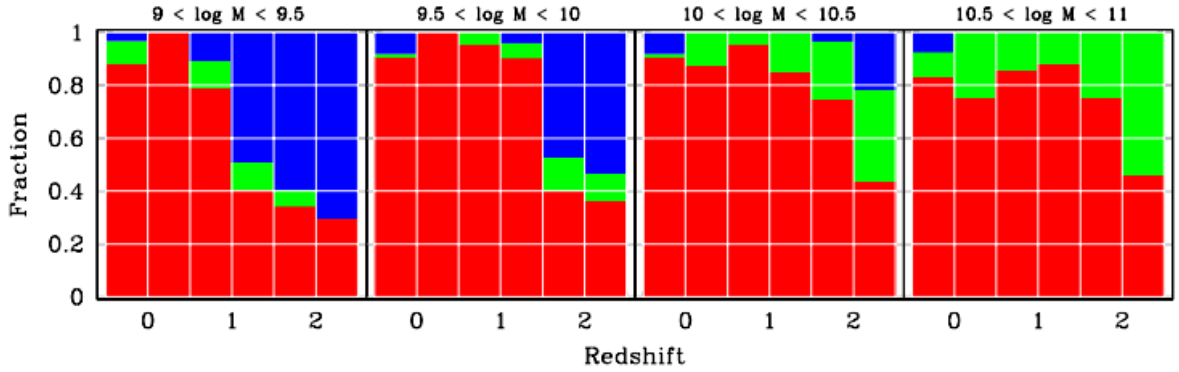

Figure 3: The fraction of each galaxy's inferred 3-D shape is indicated in colour as a function of redshift and stellar mass (van der Wel et al., 2014).

Although more and more $z > 6$ galaxies are being discovered, there are relatively

more observational data on galaxies at $z < 3$. Much effort has been devoted on analyzing galaxies in this redshift range to gain understanding of the physical processes responsible for their evolution as well as relating them to cosmological theory. Theoretically, we are now able to simulate cosmic objects in 3-D and high resolution at various scales. But their correctness depends upon whether the simulations are in agreement or not with observations, which is the main motivation of this study: to perform analysis on simulated galaxies from cosmological simulations in a way that will enable us to make systematic comparisons with real galaxies. In particular, we are interested in seeing whether simulated galaxies evolve geometrically the same way as those observed by CANDELS via structural parameters Sérsic index, size, and axis ratio measured from our star-forming galaxies generated from simulations.

1.2 Simulations

When dealing with galaxy evolution over cosmic time, cosmological simulations have provided insight about the physical processes that occurred at different epochs which can be observationally difficult or impossible to attain. Image resolution of higher redshift galaxies is generally quite low and thus their morphological properties are less known in comparison to galaxies in the local Universe. Because structural and morphological evolution took place at higher redshifts as indicated by the deviation of high redshift galaxies from the Hubble sequence (due to high SFR, mergers, etc), in this study we focus on analyzing the global properties of star-forming galaxies at $1 < z < 3$. The star-forming galaxies from 3-D cosmological simulations are generated using the Adaptive Refinement Tree (ART) code with resolution 17-35 pc (Ceverino et al., 2014). It assumes the standard ΛCDM cosmology with the WMAP5 cosmological parameters. There are a total of 3 generations of simulations: VELA, VELA_v2, and VELA_v2.1, respectively. For this work we consider the second (VELA) and third (VELA_v2) generation. Each of the galaxy evolves from the initial conditions that the dark-matter haloes generated at lower resolution have viral masses within the range of $10^{11} - 10^{12} M_{\odot}$ and that they do not show to have ongoing mergers $z = 1$ (Ceverino et al., 2014). Galaxies are then simulated using the selected dark-matter haloes in high resolution down to $z \sim 1$. The second generation of simulations (VELA) incorporates the physics of cooling, star formation, and thermal stellar feedback from supernovae and stellar winds, as implemented in basic galaxy formation simulations without any types of radiative pressure (RP) feedback. These galaxies overproduce stars too early resulting in stellar masses to be $\sim 3-10$ times the $M\star/M_{halo}$ ratios from abundance matching methods for a given halo mass (Moody et al., 2014). The third (VELA_v2) generation includes RP

feedback mechanisms modeled as a non-thermal pressure acting only in dense, star-forming regions. These processes suppress star formation by the effect of cooling and heating of gas in the interstellar medium (star forming regions) due to UV light and stellar wind emitted by massive, young blue stars, and is a crucial mechanism for simulation to generate representative galaxies as seen in the Universe. Galaxies with RP result in stellar mass-to-halo mass ratios more similar to those from abundance matching estimates, at about 50% closer than those that are model without RP (Behroozi et al., 2013).

From previous studies on active star-forming regions (blue clumps) in star-forming galaxies, detailed measurements from observation by HST have shown that at z >1, star-forming galaxies have giant clumps of gas and young stars and they contribute about 30% of total SFR, where individual clumps at $z \sim 2$ contribute about 10% of total SFR (Guo et al., 2015). In terms of cosmological simulations, previous studies on VELA and VELA_v2 have shown that the number of star-forming clumps below the threshold of $M_{clump}/M_{disk} \leq 5\%$, where $M_{disk} \lesssim 2 \times 10^{10} M_{\odot} h^{-1}$, are reduced in VELA_v2 when compared to VELA (Moody et al., 2014). Furthermore, SFR in VELA is ~ 5 times higher than observation, ~ 2 times higher for VELA_v2, with stellar mass systematically higher than VELA_v2 at $z \sim 1$ and $z \sim 2$. Since overproduction of stars in cosmological simulations decreases when RP feedbacks are incorporated, for this study we also investigate the structural and morphological effects on simulated galaxies when generated with various RP feedback through systematic comparisons between the 2 generations, which is another motivation for this thesis.

In order to utilize simulated galaxies to understand observational data, the high resolution 3-D galaxies need to have visual quality comparable to those of the observed CANDELS images. The projection at various angles and the light distribution after adding dust are calculated via SUNRISE radiative transfer code. There are 6 different projected angles: 4 random angles, 1 face-on view, and 1 edge-on view, which are defined by their angular momenta. The projected images are further degraded by added noise and re-pixelated with lower resolution comparable to CANDELS images, a process called CANDELization. The parameters Sérsic index, size, and projected axis ratio of the CANDELized galaxies are obtained via GALFIT, an algorithm for analyzing 2-D digital images. These parameters are used for statistical analysis at various redshifts and stellar masses, and the goal is to determine whether our star-forming simulated galaxies exhibit the same types of evolution as seen in analysis of galaxies from CANDELS. The ability to view our projected simulated galaxies in 3-D also allows us to inspect and determine their intrinsic shapes and thus verifying inferred shapes from previous studies.

2 Methods

2.1 Sunrise and CANDELization

In order to compare simulated images with images from CANDELS, the image resolution simulated galaxies needs to match with the low resolution images of real galaxies. In the presence of dust, light emitted from within the galaxy interacts with the interstellar medium through absorption, scattering, and re-emission, causing the observed light profile to be different than it would have been in the absence of dust. This light distribution altering effect is accounted by the SUNRISE Monte-Carlo radiative transfer code which calculates the light distribution of the galaxy at various wavebands after absorption, scattering, and re-emission. (Jonsson, 2006). The outputs from SUNRISE are the projected 2-D images with the effect of dust at various wavebands and angles. These simulated images are re-pixelated to pixel scale of the detector and are convolved with the point spread function (PSF) to match the resolution of WFC3 at each waveband. Furthermore, the background noise found in CANDELS images are also added to our simulated images. These processes are known as CANDELization and the resulting images of simulated galaxies are of visual quality that highly resemble CANDELS's images. Fig. 3 shows a galaxy in H band, before and after CANDELIzation.

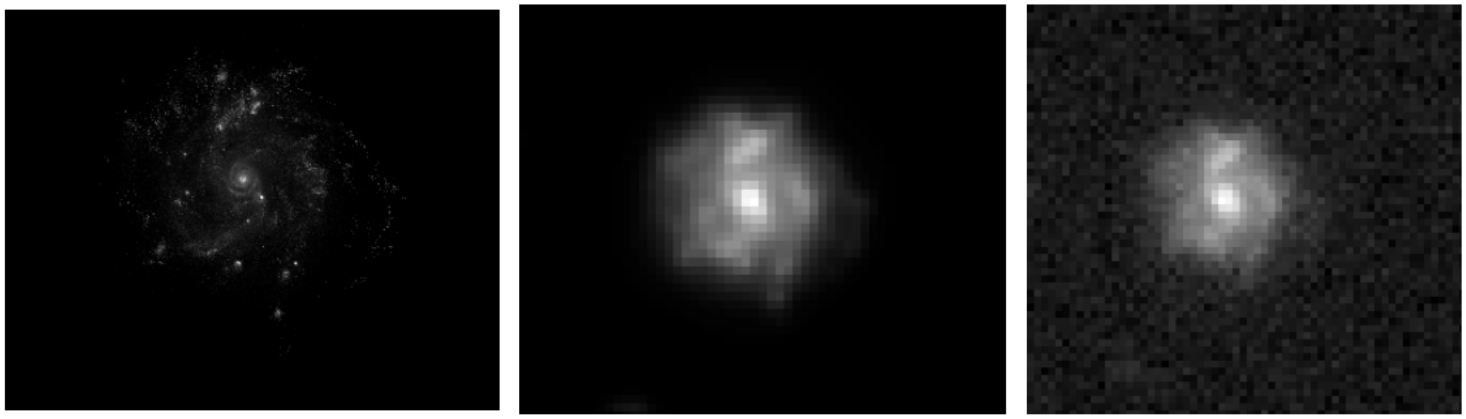

Figure 4: *Left*: A face-on view of a galaxy in high resolution in H band. *Center*: Result after SUNRISE and PSF. *Right*: Final result of CANDELization after adding background noise is very similar to images obtained from CANDELS's observation.

2.2 GALFIT

To test the representativeness of our simulations, the morphological analysis of CANDELized images is performed identically as with real galaxies observed by the HST. We apply the least-square fitting data analysis algorithm GALFIT to study the galaxies' structural components based on their light distribution by fitting 2-D digital images with a model created by the 2-D analytic function. A single model can be used to fit a single object or multiple objects simultaneously within an image. Depending on the structure complexity in terms of light distribution of the object(s), multiple models can also be created with various functions to fit different components of the galaxy or galaxies in the image simultaneously. These functions include exponential disk, Sérsic, de Vaucoulerus, Nuker, Gaussian, PSF, SKY, and a few others. Each function has adjustable free parameters to accommodate variation in galaxy shape and can be used either to create a single-component fit or in combination to create multiple-component fits (Peng, 2007). Because of the lower resolution in the CANDELized images, in this study we use the radial light profile function Sérsic to create a single-component model fitting for global morphological measurements using the parameters associated with the Sérsic function.

2.2.1 Initial Parameters

Prior to fitting, object fitting parameters must first be specified by the user to GALFIT. Our CANDELized galaxies are all fitted automatically using IDL scripts and the value for each parameter is estimated based on the single-component fit model we have chosen. GALFIT uses these estimated values to start the fitting process but the best fit value for each parameter is found by iteration based on least-squares minimization and statistics. Since these values serves only as a general prescriptions for initial 'guesses', and that GALFIT is quite insensitive to these initial parameters with the Sérsic model, they can thus be approximated based on the number of components and model used for fitting (Peng, n.d.b). Parameters can be held fixed in which the value provided the by the user remains the same during the fit, or can be set as free parameters in which case GALFIT determines the best fit value from iteration.

For the Sérsic model, the relevant object parameters are: Sérsic value n, axis ratio b/a, effective radius R_{eff}, and sky background. Assigned as free parameters for this study, GALFIT determines their value of each galaxy through least-squares minimization. The

goodness of fit is determined by the following equation

$$\chi^2_\nu = \frac{1}{N_{dof}} \sum_{x=1}^{nx} \sum_{y=1}^{ny} \frac{(f_{data}(x,y) - f_{model}(x,y))^2}{\sigma^2(x,y)} \tag{1}$$

by iterating (varying object parameters) until the best solution (lowest possible value χ^2_ν) is obtained, with an excellent fit being $\chi^2_\nu \sim 1$. The value of N_{dof} is given by the difference between the number of free parameters in the fit and the number of pixels $nx \times ny$, and is generally given by $N_{dof} \sim nx \times ny$ since the number of free parameters is much less than the number of pixels. The $f_{data}(x,y)$ is provided by CANDELized images, namely, the input data at pixel (x,y), and GALFIT generates $f_{model}(x,y)$ during the analysis based on the model created. The $\sigma(x,y)$ in the denominator is the standard deviation of the flux at pixel (x,y) known as the sigma map (Peng, n.d.a). The uncertainties associated with each of the parameter are also given by GALFIT for each fit.

A sigma map (σ image) is a map containing information about the uncertainty from counting statistic as well as changes in flux from pixel to pixel in the data image, required by GALFIT for proper fitting. Given by the Poisson statistics with Gaussian weights σ, the sigma image is essentially a noise map of the CANDELized image and is used in calculating χ^2 in Equation 1, the sum of deviation between the average value of flux of data image and the model, which GALFIT minimizes to obtain the best fit parameters. It can be generated by GALFIT or provided by the user; every CANDELized (data) image has its own corresponding sigma image. In this study, we create the σ images from the pre-calculated mode and sigma values for the sky background. There are a few things to note when one creates their own σ images. First, both the σ and data image must have the same units. Second, the units of data image needs to be converted into electrons first, and sum the uncertainty at each pixel with that due to the sky background in quadrature. And lastly, convert the electrons back to the units of data image. Since our data image is in units of [counts sec$^-$1], the uncertainty from the source is given by

$$\begin{aligned} source\ uncertainty &= \sqrt{\Big((data\ image - skymode) \times T_{exp} \times GAIN\Big)^2} &(2)\\ &= \sqrt{\Big((source) \times T_{exp} \times GAIN\Big)^2}, &(3) \end{aligned}$$

where T_{exp} is the exposure time in [sec], $GAIN$ in [electrons counts^{-1}], and data image in

[counts sec^{-1}]. The uncertainty due to the sky background is given by

$$\begin{aligned} sky\ background\ uncertainty &= [\sigma_{SKYrms} \times T_{exp} \times GAIN]^2 \quad (4) \\ &= [\sqrt{\sigma_{SKY}} \times T_{exp} \times GAIN]^2, \quad (5) \end{aligned}$$

where σ_{SKY} is in [counts]. Summing everything in quadrature:

$$\sigma\ image = \sqrt{(\sigma_{SKYrms} \times T_{exp} \times GAIN)^2 + \sqrt{(source \times T_{exp} \times GAIN)^2}}. \quad (6)$$

To convert electrons back to [counts sec$^-$1] we divide Equation 6 by $T_{exp} \times GAIN$, provided that we set $GAIN\ = 1$ giving one electron per count and the exposure time is set to $T_{exp} = 3000s$. The CANDELized images are feed to GALFIT together with the σ images.

Aside from supplying data and σ images, there are image parameters that should be specified by the user (like the initial object fitting parameters). These parameters are the convolution box size and zero point. The convolution box size is set such that the component of the galaxy being fitted is centered on the model, allowing the centre of the component to be convolved with the PSF. The values of zero point are used by GALFIT in calculating the models surface brightness in physical magnitude by converting pixel values and fluxes using the magnitude zero point specific to each waveband:

$$surface\ brightness = -2.5\ log_{10}\frac{ADUs}{T_{exp}} + magnitude\ zero\ point, \quad (7)$$

where the values of zero point can be obtained from the Hubble Space Telescope WFC3 Photometric Zeropoints webpage (http://www.stsci.edu/hst/wfc3/phot_zp_lbn).

2.2.2 Output Parameters

Output data consists of best fit object parameters and 3 images: region of input image of size specified in convolution box, image of the model used for fitting, and the residual map created by subtracting the two images. The residual image serves as a good indication of whether or not the image was fitted properly. Visual inspection of the residual map is generally motivated by strange results or suspicion about bad fitting due to other objects being fitted, and generally speaking a good fit is reflected as having minimum residual.

The best fit object parameters (Sérsic value n, axis ratio b/a, effective radius R_{eff}, and sky background) obtained from least-squares minimization are used to statistically

determine the morphological (via b/a and R_{eff}) and structural (via n) evolution of our star-forming simulated galaxies at various redshifts and stellar masses. The axis ratio of the galaxy is defined as the ratio between the semi-minor axis b and semi-major axis a of an ellipse. Roughly speaking, a galaxy in the 2-D image appears to be circular for a high axis ratio, e.g., $b/a \gtrsim 0.8$ and elongated for a low axis ratio, e.g., $b/a \lesssim 0.4$. For a more precise description, we inspect the axis ratio at different viewing angles, where the galaxy's overall 3-D geometry can be inferred via systematic comparisons between the face-on and edge-on angles, while the axis ratio of random projections represents observational statistical data. The effective radius R_{eff} given in pixel units by GALFIT is defined such that it contains half of the total luminosity from the galaxy, e.g., the radius is the semi-major axis containing half the luminosity in the ellipse of the best-fit model created by the Sérsic function. It measures the radial light distribution and is sometimes referred to as the size of a galaxy or the half-light radius of the galaxy.

The sky background accounts for the source of noise in the data image; the Sérsic function is a radial profile function that describes radial changes in intensity of a galaxy from the centre. The functional form

$$\Sigma(r) = \Sigma_{eff} \ \exp\Big[-\kappa\Big(\Big(\frac{R}{R_{eff}}\Big)^{\frac{1}{n}} - 1\Big)\Big] \tag{8}$$

gives the pixel surface brightness at radius R. Σ_{eff} is the pixel surface brightness at R_{eff}, n is the Sérsic index, and κ is a dependent variable coupled to n (Peng, 2007). The value of n describes the size and brightness of a galaxy based on the radial flux distribution. A large value in n corresponds to high brightness concentration at small radius whicth decreases steeply due to large extension of outer wing, as in elliptical galaxies with n=4. When n=1 the Sérsic function is the exponential disk profile, corresponding to galaxies of spiral, bulge-less disk like structure, where the brightness concentration at small radius is less dramatic and relatively constant throughout from center to edge. In other words, the less radial fluctuation in density from the centre, the lower the value of n. Figure 4 below shows how the intensity changes radially at various radii and the corresponding Sérsic values.

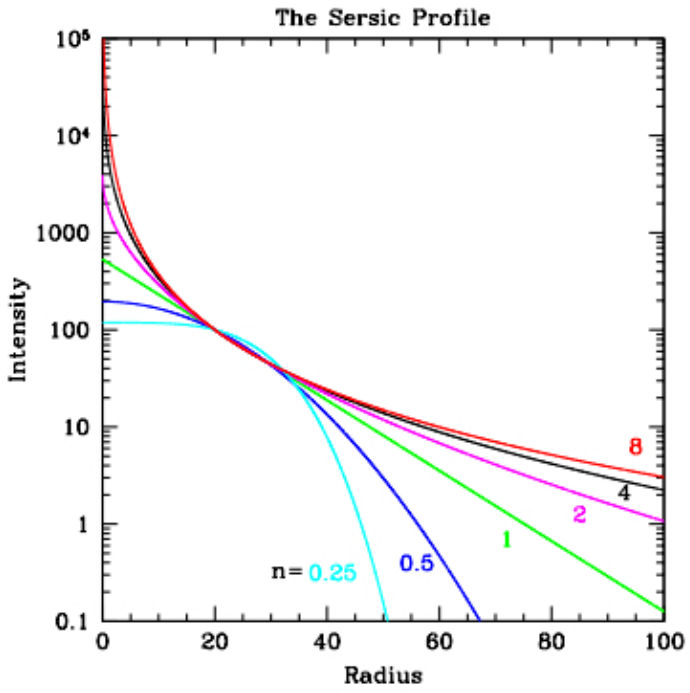

Figure 5: Surface brightness density at various r and values of their Sérsic index (Peng, 2007).

2.3 Galaxy Selection

The studies of geometrical evolution of CANDELS star-forming galaxies as described in §1.2 were observed in optical (F775W) and NIR (F160W) wavebands. Since our goal is to make systematic comparison with our simulated galaxies to those of CANDELS, for this study we select our simulated galaxies at $1 \lesssim z \lesssim 3$ in band F160W for the analysis. As discussed in §1.3, for each generation there is a total of 35 simulated galaxies, each simulated with identical initial conditions is expected to evolve differently. Although the galaxy's star-forming history dictates its evolution, at a particular time-step (redshift) the galaxy is considered to be statistically independent from the rest. Each analysis is repeated three times: we analyze the best fit parameters given by GALFIT for face-on, edge-on, and random viewing angles separately. Note that GALFIT provides the uncertainties associated with best-fit parameters, and typically they are within the acceptable values. However, in some cases GALFIT may have fitted certain images poorly, giving large uncertainty for one or multiple parameters. In this case, we exclude their data points in our plots and investigate for possible problematic images or initial parameters (see §3.4). Also note that the follow up analysis on results presented in this study involving random angels show that these angles are not truly random. Although the nature of these supposed random angles has not been

determined except that each of the 4 random angles are appears to be the same angle at every time-step, we note here that in the following discussions we take this into account and thus all results due to random viewing angles should not be used for inferring shapes as they do not represent random distributions. On the other hand, images of galaxies for simulation 28 are seen to be elongated at higher redshifts in which the elongation is reflected in the random plot. Thus, in the following discussion we include observations from random plots for simulations that exhibit strong trends of elongated galaxies, reserving the possibility that the random plots may be good indications provided that we verify how these angles are projected (for future work).

Of the 3 generations and the 35 simulations available per generation, we have chosen a total of 5 simulations each for generations VELA and VELA_v2 for this study. The VELA_v2 generation is refer to as VELAxxMRP within the plots, where xx is the name of the simulation (i.e., 02, 04, etc). Table 1 below lists the simulation names and stellar masses for VELA_v2 at $z \sim 1$ and $z \sim 2$ (Snyder et al., 2014); since galaxies of VELA are systematically more massive and overproduce stars more than galaxies of VELAxxMRP, we use the stellar mass of VELA_v2 for shape comparisons as they resemble more realistically CANDELS galaxies.

Simulation	$M_\star$ at $z \sim 2$ $\log_{10} M_\star/M_\odot$	$M_\star$ at $z \sim 1$ $\log_{10} M_\star/M_\odot$
VELA02MRP	9.4	10.0
VELA04MRP	9.2	9.6
VELA05MRP	9.3	9.6
VELA27MRP	10.0	10.3
VELA28MRP	9.5	9.8

Table 1: Simulations with RP feedback and their corresponding stellar masses at $z \sim 1$ and $z \sim 2$.

3 Data and Analysis

3.1 Axis Ratio and Sérsic

We begin by looking at how the axis ratio b/a evolves as a function of redshift for each of the 5 simulations. Each data point is coded with various symbols to indicate its corresponding Sérsic index (n) (within a certain interval). The intervals are defined in the following way:

Sub-disk (Elongated)	Disk	Disk-Spheroid	Spheroid
$n < 0.8$	$0.8 \leq n < 1.5$	$1.5 \leq n < 2.5$	$2.5 \leq n < 5$

Table 2: Sérsic indices and their corresponding shapes.

By dividing up Sérsic values into intervals the distinction between small spheroids and elongated objects becomes more apparent. When viewed face-on, disk-like galaxies have high axis ratios ($\gtrsim 0.7$) and Sérsic values corresponding to exponential light profile ($n \sim 1$); when viewed edge-on, the axis ratios are low ($\lesssim 0.4$) with Sérsic values similar to that of face-on. For elongated galaxies, the axis ratio should be low ($\lesssim 0.5$) when viewed edge-on and high when viewed face-on (looking down along the long axis), similar to that of disks. For spheroidal galaxies, their axis ratios and Sérsic values remain high at all angles. Because elongated and spheroidal objects both have high axis ratio when viewed face-on, we attempt to distinguish them via the small and high Sérsic values respectively. Furthermore, the 3-D geometries are first inferred by studying the face-on and edge-on plot, in which our assumptions are expected to be reflected in the random viewing angle plots. For example, if we suspect the simulation to be a disks at lower redshifts, then this should be reflected in the random plot where in the same redshifts the data points are distributed evenly across all axis ratios. If the simulation seems elongated at higher redshifts, then this should be reflected in the random plot with data points clustering towards lower value of axis ratios.

In the following section, Figures 6 to 10 show plots of axis ratio vs. redshift where data points of simulation with RP (VELAxxMRP) and without RP (VELA) are combined on a single plot for comparisons, follow by discussions of the results. Although number of data points of VELA are much less than VELAxxMRP due to fewer timesteps saved for the VELA simulations (aside from exclusion due to large uncertainties), the difference in axis ratio evolution between the two can be seen quite clearly in most cases (at all viewing angles). For example, even though the axis ratios are similar between the two, their corresponding n

values can be quite different at some redshift interval. This is no surprise as we have stated that galaxies generated without RP are found too be producing stars to quickly at early times resulting in overly massive galaxies. This high SFR would in turn to have different morphology of the same galaxies generated with RP. In the discussions below we note that this has been observed. Note that except for VELA27MRP at $z \sim 2$, all RP simulations considered are within the lower-mass range (10^9 to $10^{9.5} M_\odot$) which (van der Wel et al., 2014) have shown that at $1 < z < 2.5$ a majority of the galaxies within this stellar mass range are elongated. Also note that, except for VELA27MRP at $z \sim 1$, all RP simulations considered here are within the mass range ($10^{9.5}$ to $10^{10} M_\odot$), which (van der Wel et al., 2014) have show that at $1.5 < z < 2.5$ a majority of the galaxies within this stellar mass range are also elongated. From these observations, we suspect that similar findings can be found from the same types of galaxies generated with RP; simulations that are found to be in agreement with these observations will be stated within the discussion.

3.1.1 Discussion

- VELA02MRP has a stellar mass of $10^{9.4} M_\odot$ at $z \sim 2$ and $10^{10} M_\odot$ at $z \sim 1$; VELA02 is more massive than VELA02MRP. For VELA02MRP, in the face-on view we see the $b/a \sim 0.7$ at $z \sim 2$ and in edge-on view $b/a \sim 0.5$, indicating that these galaxies are elongated at these redshifts. This is supported by that most $n < 0.8$ in the edge-on view. Give that b/a increases towards lower redshifts as seen in the edge-on view, elongated galaxies at higher redshifts are likely to evolve to structures that are between disks and spheroid at lower redshifts. VELA02 have similar evolution at $z \sim 2$. Broadly speaking, however, galaxies in VELA02 are seen to evolve differently than VELA02MRP at all redshifts. And the over all evolution of axis ratios across $1 < z < 2.5$ for VELA02MRP shows that they started out elongated and evolve to spheroids, and not disks, due to the high axis ratios at $z \sim 1$. Given the stellar mass at $z \sim 1$ and $z \sim 2$, VELA02MRP exhibit the same properties and those in CANDELS (elongated at higher z).

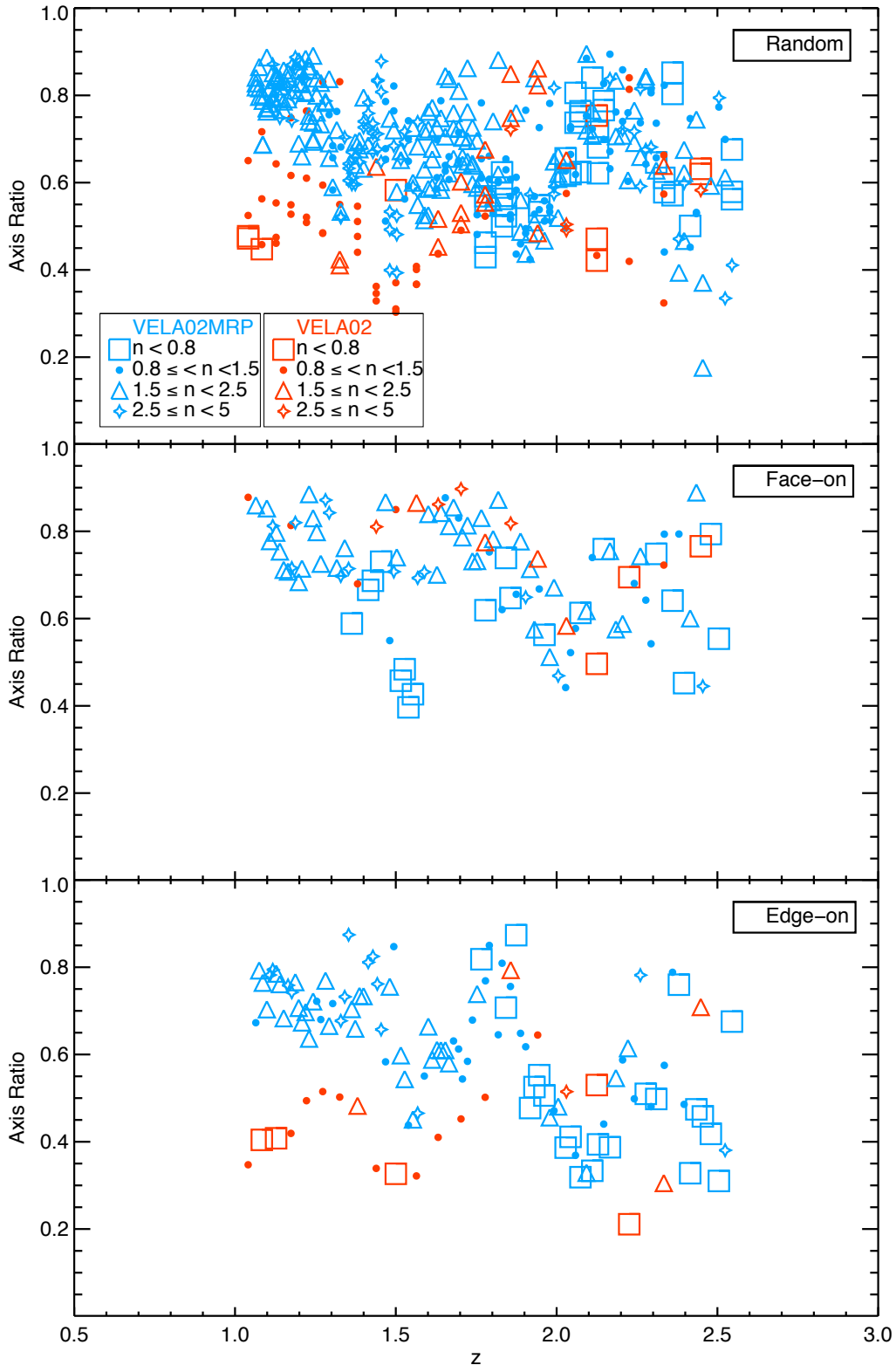

Figure 6: VELA02 AND VELA02MRP

- VELA04MRP has a stellar mass of $10^{9.2} M_{\odot}$ at $z \sim 2$ and $10^{9.6} M_{\odot}$ at $z \sim 1$; VELA04 is more massive than VELA04MRP. At $1.5 < z < 2.5$ axis ratios of VELA04MRP increase significantly from ~ 0.2 to ~ 0.8 where their corresponding Sérsic values remain low (< 0.8). At the same redshifts, there exist broadly distributed axis ratios and Sérsic indices when viewed edge-on, making these galaxies appears to be irregularly shaped objects starting at $z = 2.5$, and evolve to a mixture of shapes as redshift decreases; at $1 < z < 1.5$, $b/a \sim 0.8$ in face-on and $b/a \sim 0.5$ in edge-on with $n > 2.5$ in both cases imply that VELA04MRP are not thin disks at low redshifts, and likely to be spheroids. At higher redshifts ($z > 1.5$) the high axis ratios (~ 0.8) in the face-on view and low axis ratios (~ 0.3) in the edge-on view suggest that VELA04 are already disks early on. The general evolution is very different between VELA04MRP and VELA04.

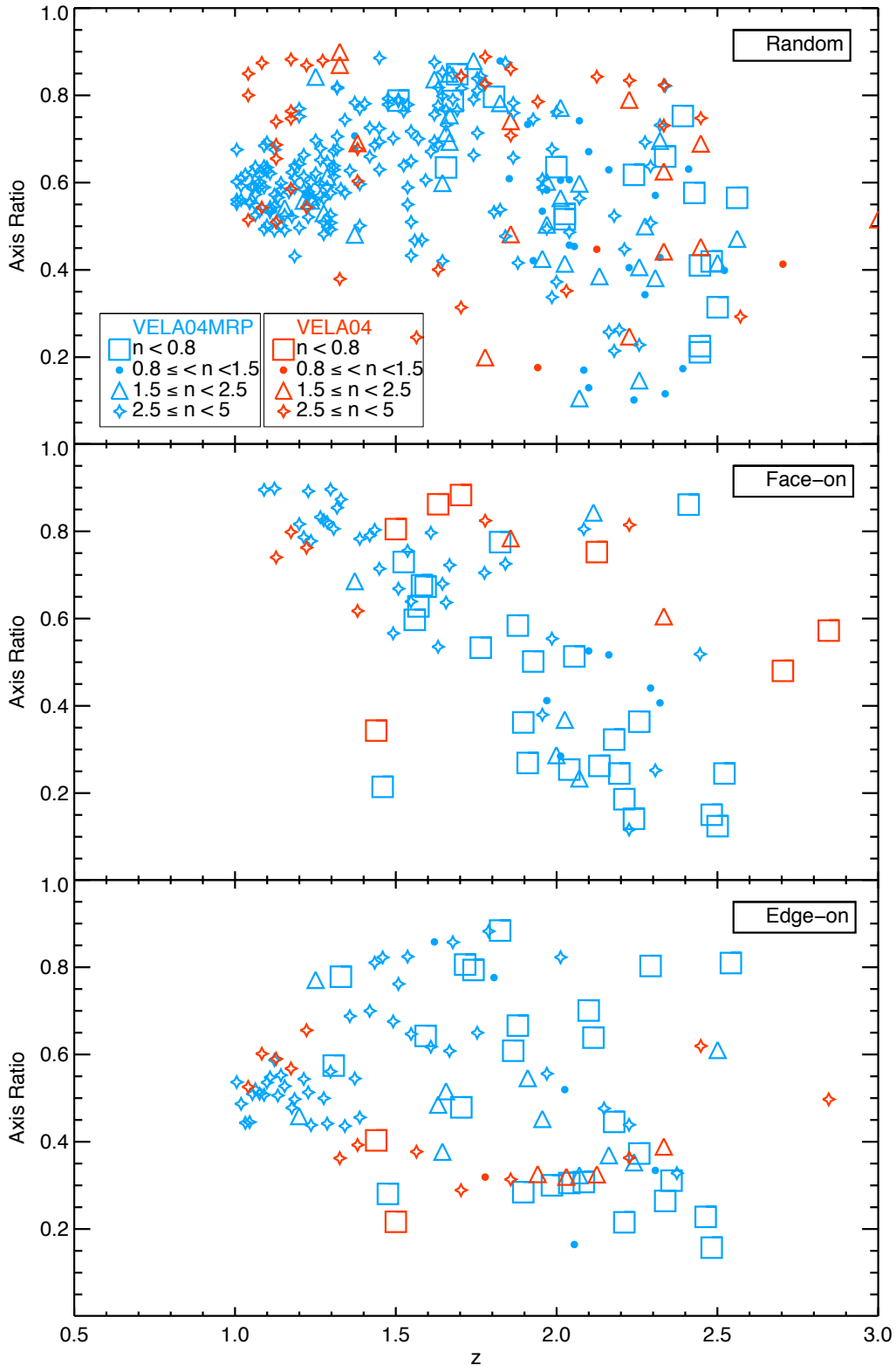

Figure 7: VELA04 AND VELA04MRP

- VELA05MRP has a stellar mass of $10^{9.3} M_{\odot}$ at $z \sim 2$ and $10^{9.6} M_{\odot}$ at $z \sim 1$; VELA05 is more massive than VELA05MRP. For VELA05MRP at $2 < z < 2.5$, low axis ratios in both face-on and edge-on view suggest that galaxies are shaped irregularly, especially at $z = 2.5$ where the $b/a \sim 0.7$ in edge-on and $b/a \sim 0.3$ in face-on. However, they become elongated between $1.5 < z < 2$ due to low b/a in the edge-on with mid-high b/a in the face-on view. Both VELA05 and VELA05MRP evolve similarly when viewed edge-on at all redshifts, and at $z < 1.5$ VELA05MRP have Sérsic values between disks and spheroids, while VELA05 are all disks ($n > 2.5$). VELA05MRP is seen to have elongated galaxies comparable to those of CANDELS at $1.5 < z < 2$ given their stellar masses and $z \sim 1$ and $z \sim 2$.

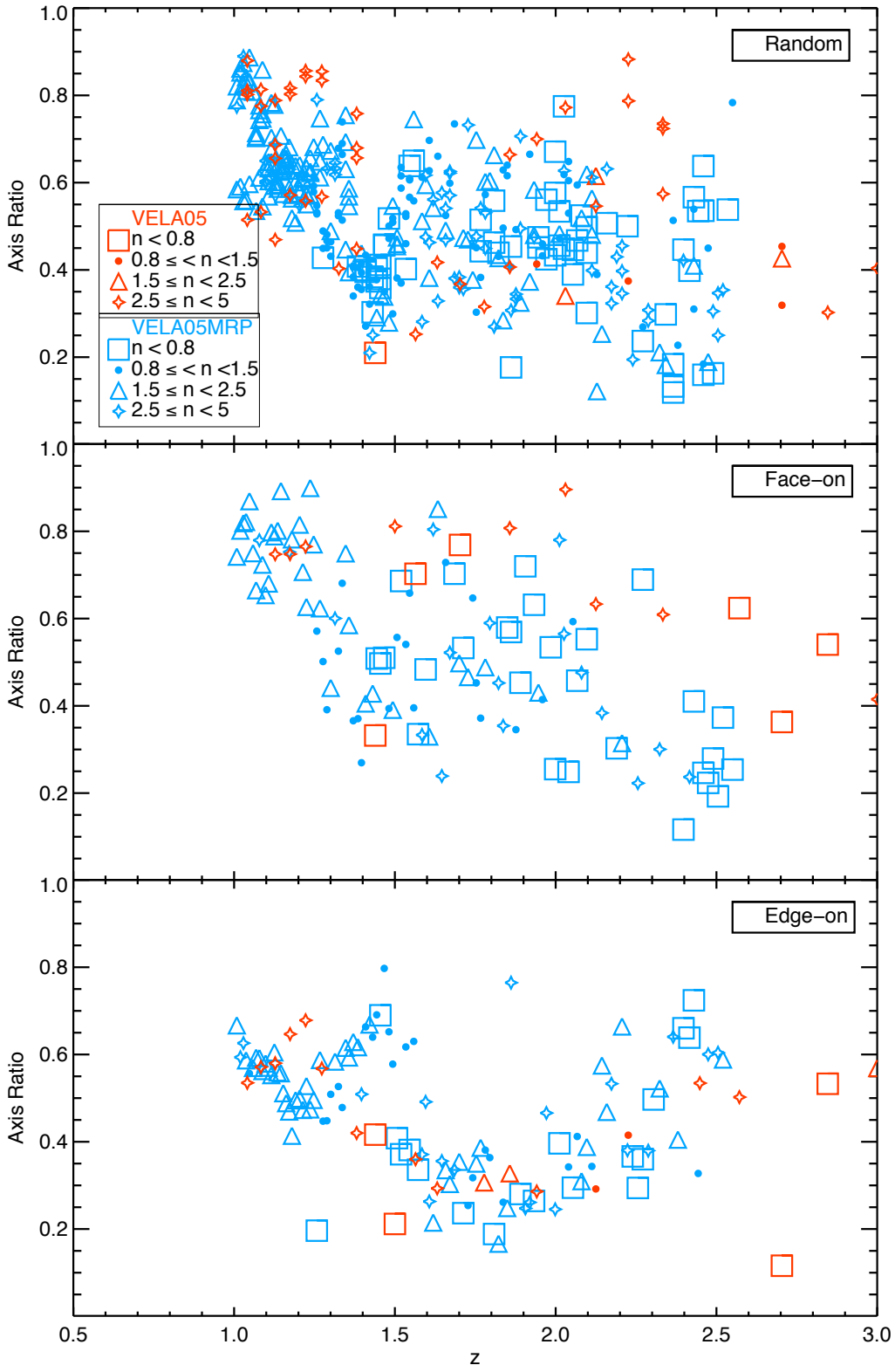

Figure 8: VELA05 AND VELA05MRP

- VELA27MRP has a stellar mass of $10^{10} M_{\odot}$ at $z \sim 2$ and $10^{10.3} M_{\odot}$ at $z \sim 1$; VELA27 is more massive than VELA27MRP. At $z > 2$, VELA27MRP appear to be a mixture of elongated and irregular galaxies given by the low axis ratios in edge-on while having a broader range near the high values in the face-on view. Their corresponding Sérsic indices also vary greatly in the edge-on view, in support of having different shapes. VELA27 on the other hand have characteristics of elongated galaxies at the same redshifts. A strong transition occurs at $z \sim 2$, where the axis ratios of VELA27MRP increase to a constant value $b/a \sim 0.9$ in the face-on view down to $z = 1$, while in the edge-on view at $1.5 < z < 2$ axis ratios have mid-values (~ 0.5), suggesting elongated galaxies. At lower redshifts ($1 < z < 1.5$) the edge-on axis ratios drop to even lower values ($b/a \sim 0.3$), suggesting that these galaxies are disks. Their corresponding Sérsic indices are also generally low. VELA27 evolve similarly as VELA27MRP, but there are no data points for VELA27 below $z \sim 1.5$ to determine their shapes. VELA27MRP galaxies are similar to those of CANDELS where they are elongated at $1.5 < z < 2$.

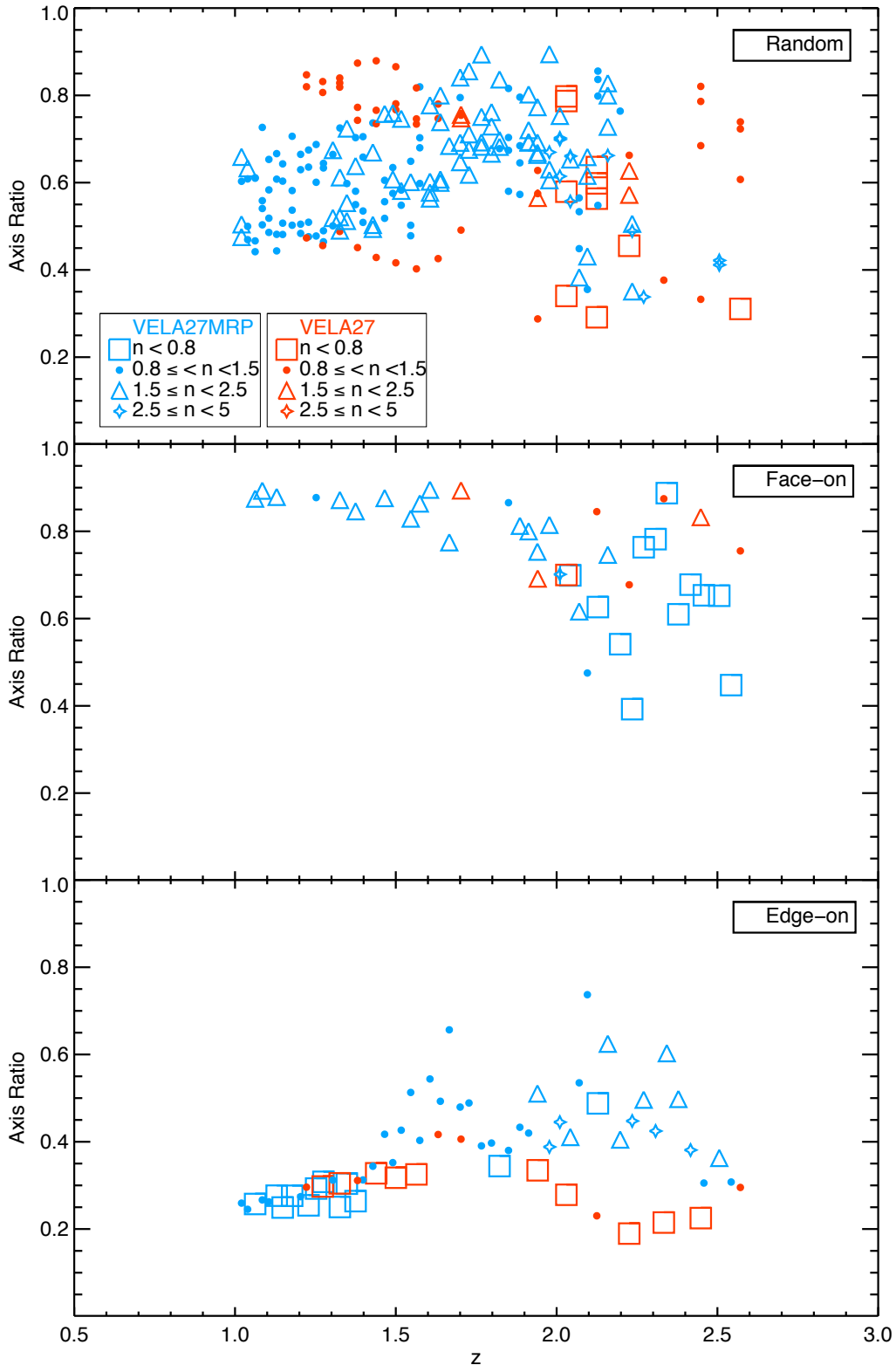

Figure 9: VELA27 AND VELA27MRP

- VELA28MRP has a stellar mass of $10^{9.5} M_{\odot}$ at $z \sim 2$ and $10^{9.8} M_{\odot}$ at $z \sim 1$; VELA28 is more massive than VELA28MRP. Galaxies of VELA28MRP appear to be irregularly shaped at $2 < z < 2.5$, given by the low axis ratios with wide range of Sérsic indices in both the face-on and edge-on views. As we go towards lower redshifts ($z < 2$), they appear to be elongated as the axis ratios increase to high values in the face-on view while remain low in the edge-on view; their Sérsic values are also generally low at these redshifts. Although the distinction between disks and elongation is not clear at $z < 2$, we expect that at $z \sim 1$ galaxies have evolve from elongated objects to disks. The evolution of VELA28 is inconclusive at higher redshifts, but at $1 < z < 1.5$ all galaxies have $b/a < 0.3$ implying that they are disks. From the about discussion, we conclude that VELA28MRP galaxies are likely to be elongated at $z \sim 1.5$.

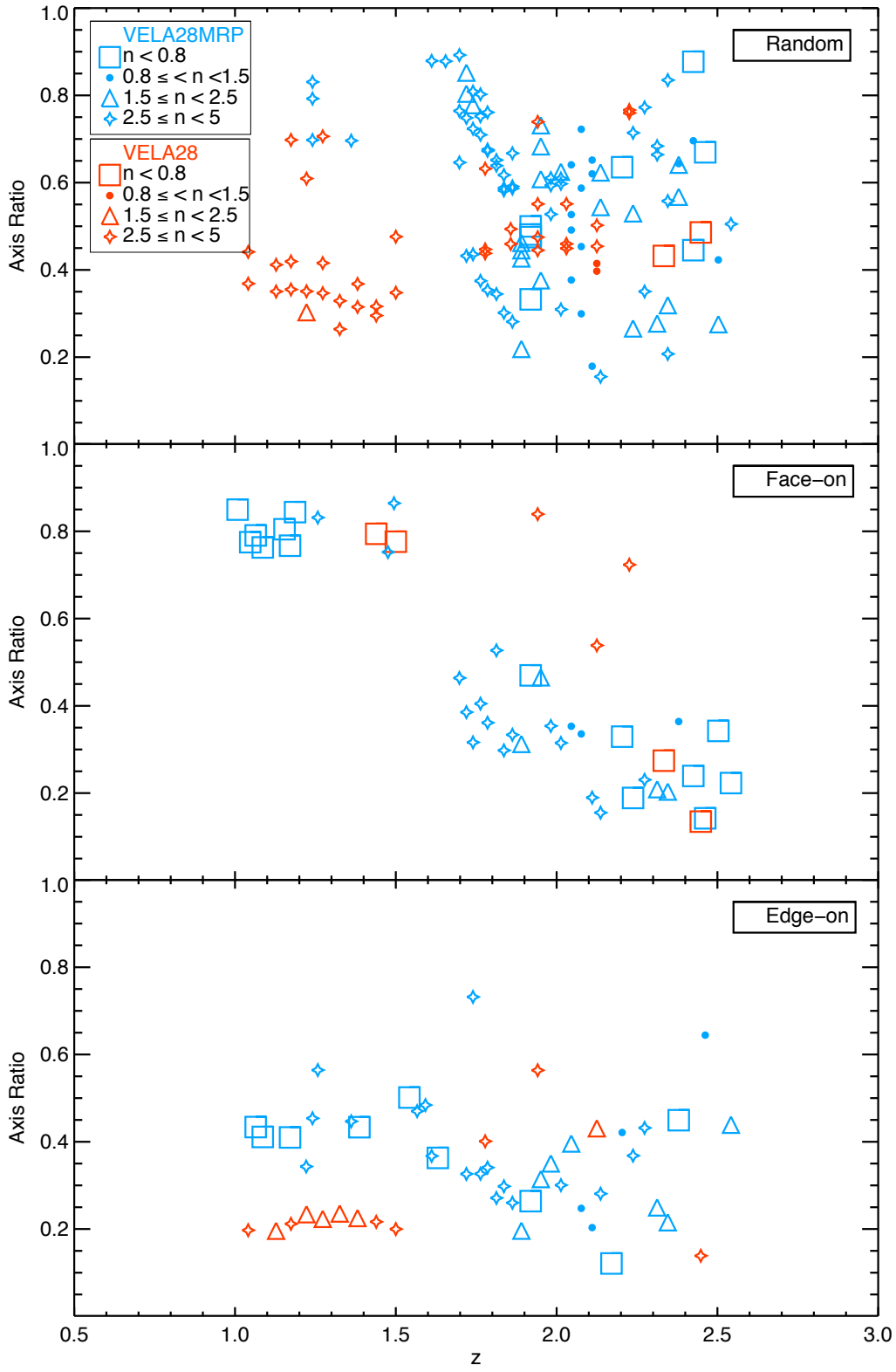

Figure 10: VELA28 AND VELA28MRP

- Due to the inability of random plots to reflect the deduced shapes from face-on and edge-on plots as these angles were found to be not truly random, and that in some cases we found difficulty in distinguishing between small disks and spheroidal structure due to the broadly distributed Sérsic indices, in the next section we present a different way of illustrating our data allowing the sizes of galaxies to be included. This improves our ability on understanding the correlation between size, redshift, Sérsic, and axis ratio. We also investigate the reliability of our random plots and the initial parameters assigned to GALFIT, and also the data points excluded from our plots due to large uncertainties given by GALFIT in §3.4 via inspecting both the high-resolution and H band images.

3.2 Shapes and Sizes

We now turn to the analysis on shapes and sizes. By plotting the Sérsic index n, effective radius R_{eff}, and axis ratio b/a in the 3-panel type plot in slices of redshifts, the shapes of galaxies can be seen more easily. Each simulation is plotted this way and is separated into face-on, edge-on, and random viewing angles. In both types of galaxies (with and without RP), we expect that disk-like structure to be dominating at low redshifts ($z \sim 1$) and elongated at $z \sim 2$, as observed in star-forming galaxies from the CANDELS survey.

3.2.1 $1 \leq z \leq 1.5$

Disk-like structure is apparent from the face-on and edge-on plots with galaxies without RP in simulation 02 (VELA02) and 27 (VELA27): low axis ratio when viewed edge-on and high axis ratio when viewed face-on, with Sérsic indices $n \sim 1$. For all other galaxies without RP (simulation 04, 05, and 28), their axis ratios from edge-on and face-on views indicate disk-like structure; however, their Sérsic indices are too high ($n > 3$) to be considered disks. Disk-like structure is seen, although less apparent since Sérsic indices are also a bit too high, from the face-on and edge-on plots of all galaxies with RP (expect for VELA27MRP which exhibits strong indications of disk-like structure). In both case, these high Sérsic indices may be a hint for disk-spheroidal objects given that their corresponding axis ratios are spread out enough in the mid-higher range ($b/a \sim 0.6$) when viewed edge-on.

The transformation from elongation to objects with structures that are intermediate between disks and spheroids can be seen quite clearly in the random plot for VELA05MRP: where the axis ratio decreases with Sérsic index, and small spheroids having high Sérsic and elongated objects having low Sérsic are distinguishable by the growth in R_{eff} with decreasing axis ratio. These observations however are not reflected in the face-on plot for at large radii the axis ratios drop below 0.6, although puzzling, as both spheroids and elongated objects are expected to have higher axis ratios in the face-on view, we note earlier that the nature of these random angles are not yet known, except that each of the 4 random angles are appears to be the same angle at every time-step. Nonetheless, the trend observed in the random plot tells us that there likely to exist elongated objects in VELA05MRP, but further investigation on what these angels are is required for better interpretation.

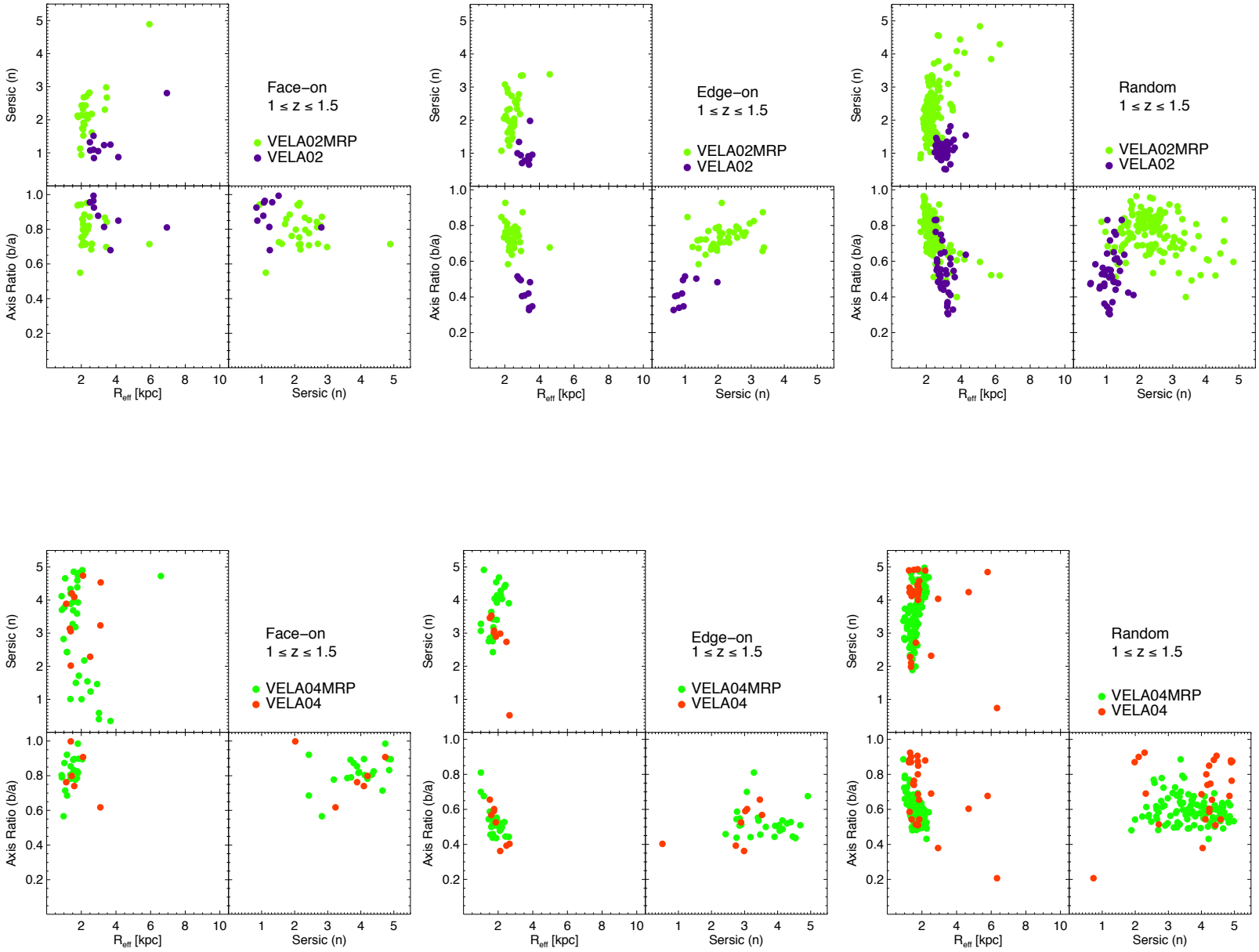
Face−on
1 ≤ z ≤ 1.5
VELA02MRP
VELA02
Edge−on
1 ≤ z ≤ 1.5
VELA02MRP
VELA02
Random
1 ≤ z ≤ 1.5
VELA02MRP
VELA02
Face−on
1 ≤ z ≤ 1.5
VELA04MRP
VELA04
Edge−on
1 ≤ z ≤ 1.5
VELA04MRP
VELA04
Random
1 ≤ z ≤ 1.5
VELA04MRP
VELA04
Sersic (n)
Axis Ratio (b/a)
R_eff [kpc]
Sersic (n)

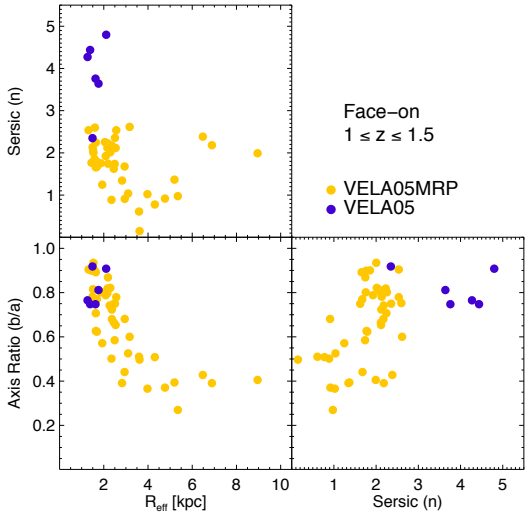
Face–on
1 ≤ z ≤ 1.5
VELA05MRP
VELA05
Sersic (n)
Axis Ratio (b/a)
R_eff [kpc]
Sersic (n)

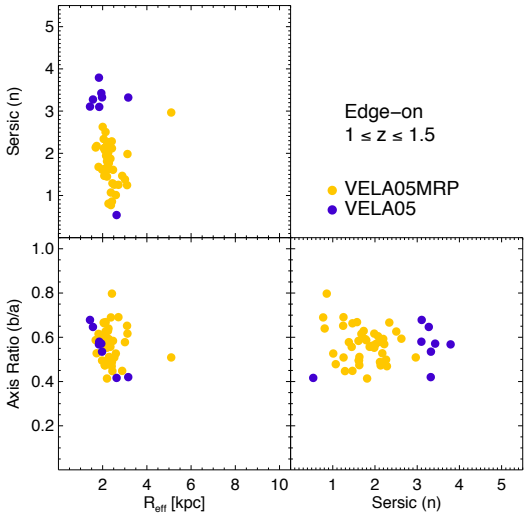
Edge–on
1 ≤ z ≤ 1.5
VELA05MRP
VELA05
Sersic (n)
Axis Ratio (b/a)
R_eff [kpc]
Sersic (n)

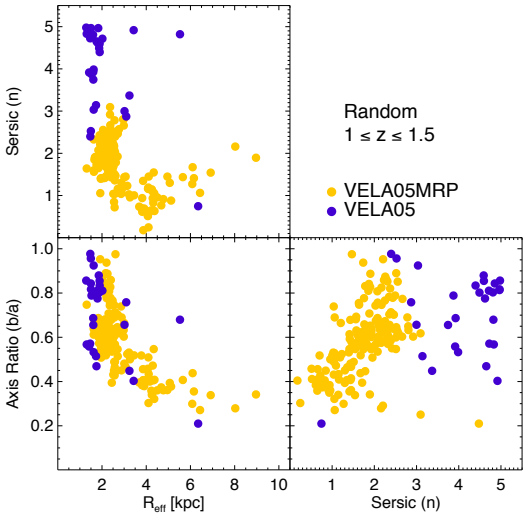
Random
1 ≤ z ≤ 1.5
VELA05MRP
VELA05
Sersic (n)
Axis Ratio (b/a)
R_eff [kpc]
Sersic (n)

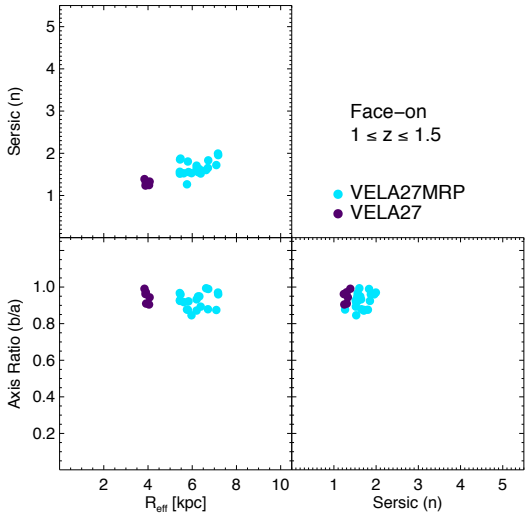
Face–on
1 ≤ z ≤ 1.5
VELA27MRP
VELA27
Sersic (n)
Axis Ratio (b/a)
R_eff [kpc]
Sersic (n)

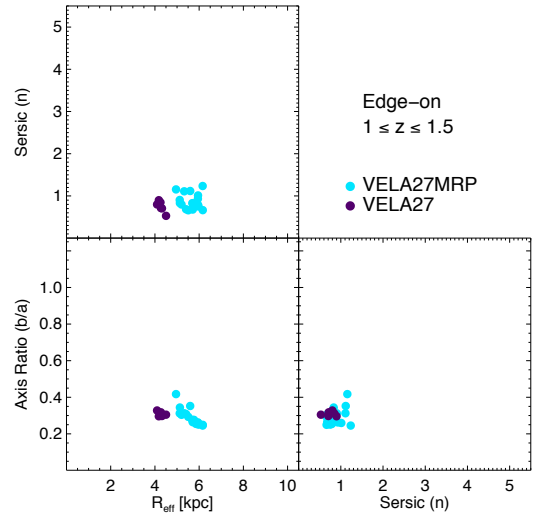
Edge–on
1 ≤ z ≤ 1.5
VELA27MRP
VELA27
Sersic (n)
Axis Ratio (b/a)
R_eff [kpc]
Sersic (n)

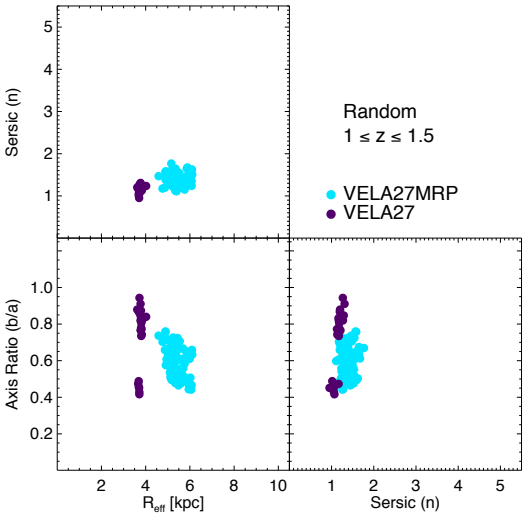
Random
1 ≤ z ≤ 1.5
VELA27MRP
VELA27
Sersic (n)
Axis Ratio (b/a)
R_eff [kpc]
Sersic (n)

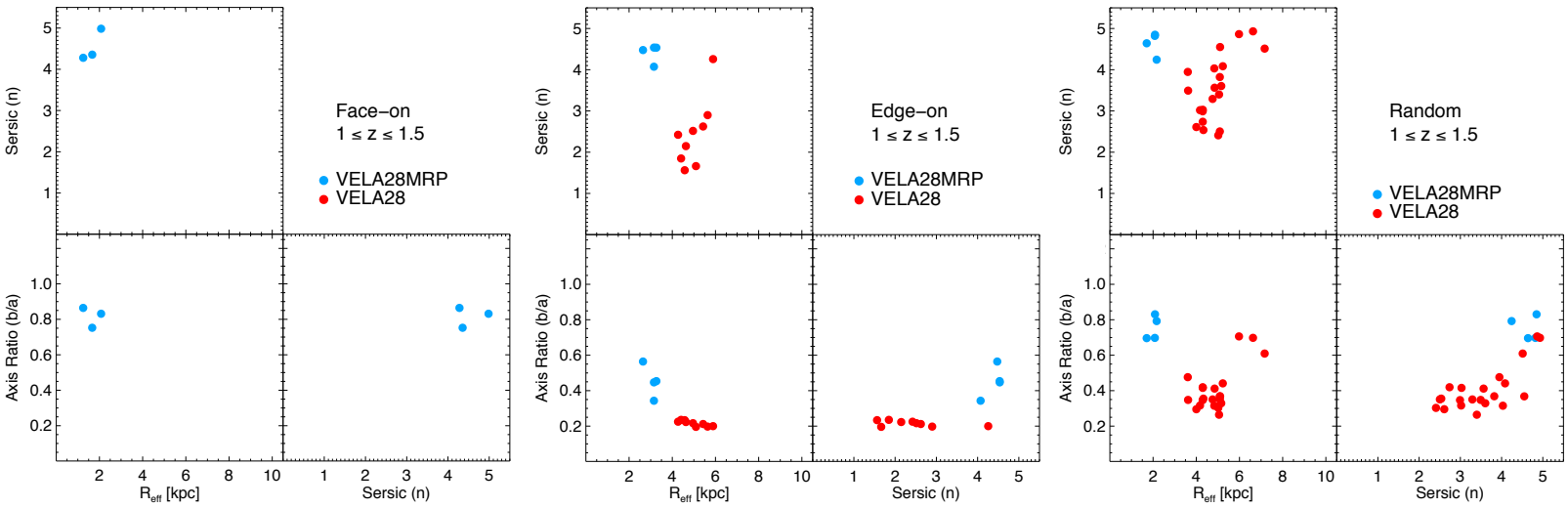

Figure 11: A three panel plot of axis ratio, R_{eff}, and Sérsic index of 5 simulations at $1 \leq z \leq 1.5$.

3.2.2 $1.5 \leq z < 2$

The axis ratios are generally high in VELA02MRP as seen in all three viewing angles. Disk-spheroid structure is implied by the decrease in Sérsic indices with axis ratios. Low axis ratios with generally low Sérsic indices at larger radii in the edge-on view with generally high axis ratios and also low Sérsic in the face-on view suggest that some of these galaxies are elongated. For VELA04MRP, although the axis ratio decreases with Sérsic index, indicating elongated objects, all radii are less than $\sim$ 2 kpc at which a wide range of Sérsic values exist, providing difficulty in distinguishing between small disks and spheroids. Very similar correlation in the corresponding face-on and edge-on plots also hint that results for this simulation should not be used in determining their shapes. VELA27MRP appears to be disk-spheroid objects: high axis ratio at all radii with Sérsic indices ranging from 1-3 in the face-on plot, and axis ratio ~ 0.5 with low Sérsic ($n < 2$) in the edge-on plot. It is worth noting that the random views also support this inferred structure given that data points cluster around high axis ratios and low Sérsic indices, but again we should be careful about how to interpret random results.

Elongated objects are seen in the random plot of VELA28MRP, where at small radii the axis ratio and Sérsic index have high values corresponding to spheroids, and at larger radii ($R_{eff} > 4$ kpc) both the axis ratio and Sérsic index drop to lower values, implying that some of these galaxies are elongated. These elongated galaxies may also be somewhat irregular as the axis ratio at R_{eff} are a bit too low ($b/a \sim 0.4$) for the ideal values of an elongated object projected along the long axis ($b/a \gtrsim 0.8$). Their face-on plot however, have axis ratios that are below the expected value for elongation. Scatter-ness in the face-on data points of VELA05MRP provides difficulty in determining elongation, but the low axis ratios as seen in the edge-on view suggest that they are likely to be elongated. There are too few data points with all galaxies without RP for conclusions to be drawn.

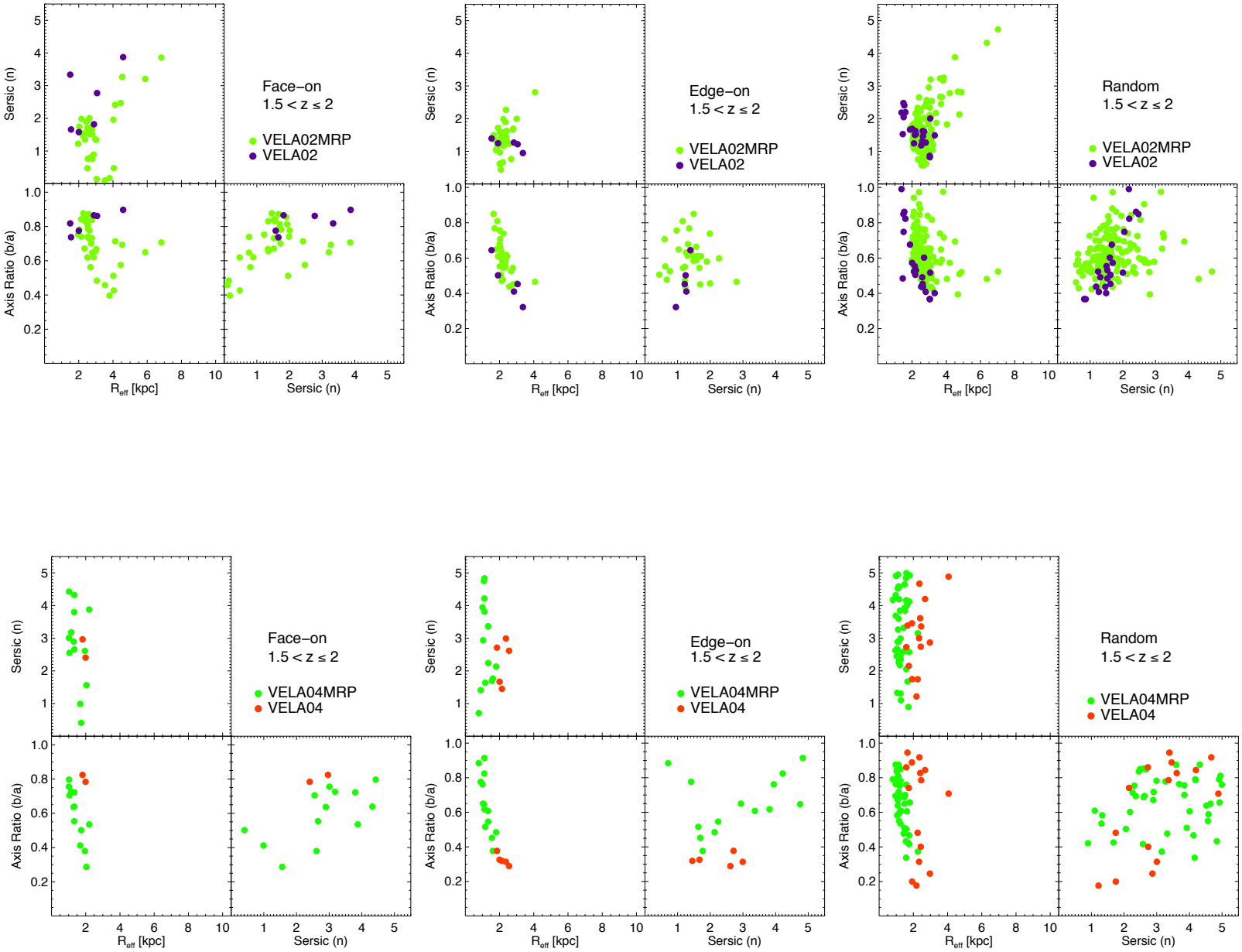
Face−on
1.5 < z ≤ 2
VELA02MRP
VELA02
Edge−on
1.5 < z ≤ 2
VELA02MRP
VELA02
Random
1.5 < z ≤ 2
VELA02MRP
VELA02
Face−on
1.5 < z ≤ 2
VELA04MRP
VELA04
Edge−on
1.5 < z ≤ 2
VELA04MRP
VELA04
Random
1.5 < z ≤ 2
VELA04MRP
VELA04
Sersic (n)
Axis Ratio (b/a)
R_eff [kpc]
Sersic (n)

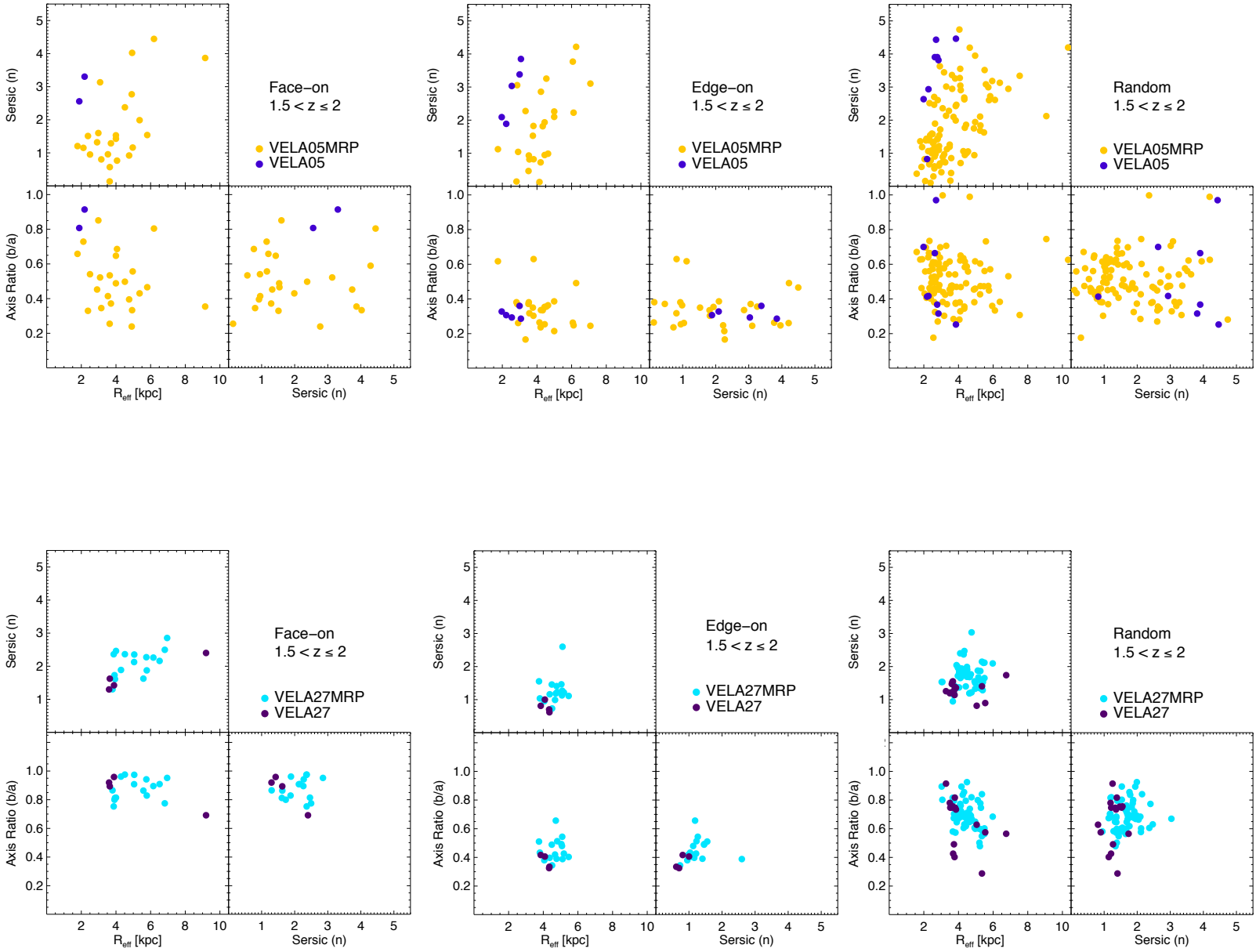
Face–on
1.5 < z ≤ 2
VELA05MRP
VELA05
Edge–on
1.5 < z ≤ 2
VELA05MRP
VELA05
Random
1.5 < z ≤ 2
VELA05MRP
VELA05
Face–on
1.5 < z ≤ 2
VELA27MRP
VELA27
Edge–on
1.5 < z ≤ 2
VELA27MRP
VELA27
Random
1.5 < z ≤ 2
VELA27MRP
VELA27
Sersic (n)
Axis Ratio (b/a)
R_eff [kpc]
Sersic (n)

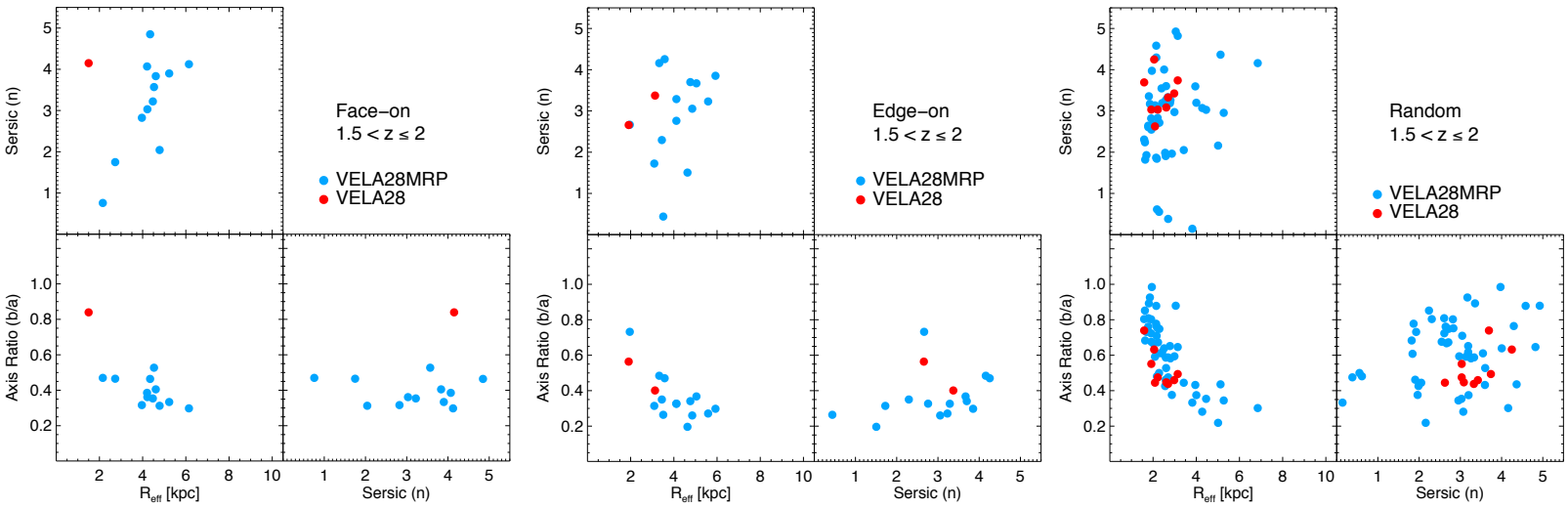

Figure 12: A three panel plot of axis ratio, R_{eff}, and Sérsic index of 5 simulations at $1.5 < z \leq 2$.

3.2.3 $2 \leq z < 3$

The first thing to notice is that plots of VELA05MRP and VELA28MRP in random viewing angles exhibit the trend one expects to see if galaxies are elongated in the axis ratio vs. R_{eff} plot. At small radii these galaxies have higher axis ratios, corresponding to small spheroids. As the size increases the axis ratio decreases, corresponding to elongated objects. However, the wide range of Sérsic indices ($0 < n < 3$) at small radii is not a good indicator on whether these star-forming galaxies are spheroidal or small disks. Another puzzling fact is that for VELA05MRP, low Sérsic indices ($0 < n < 2$) have a wide range of axis ratios, in contradiction with elongated galaxies having generally low values of axis ratios. This may be related to randomness which we have previous noted. In both cases, their corresponding face-on and edge-on analysis are not entirety supportive of elongation as the data points for each parameter are again too scattered.

For simulation 02 and 04, both with and without RP have radii $2 < R_{eff} < 4$ kpc, and at each radius there are again a wide range of axis ratios and Sérsic indices. VELA02MRP have more concentrated data points around low Sérsic indice for low axis ratios in the edge-on view while high in axis ratios in face-on view, suggesting that some of these galaxies are elongated. The number of data points is too few in the face-on and edge-on plots of simulation 27 for interpretation. Its random plot shows that the radii of galaxies with RP grow with Sérsic indices, while the axis ratios decrease with increasing Sérsic indices; it is difficult to tell what the shapes are for these galaxies. We suspect that there may be occasional minor mergers at higher redshifts ($z > 2$), which could explain some of the weird results we have seen thus far as GALFIT fits all data images using a single-component fit. In the following sections (§3.3 and 3.4) we investigate this potential issue.

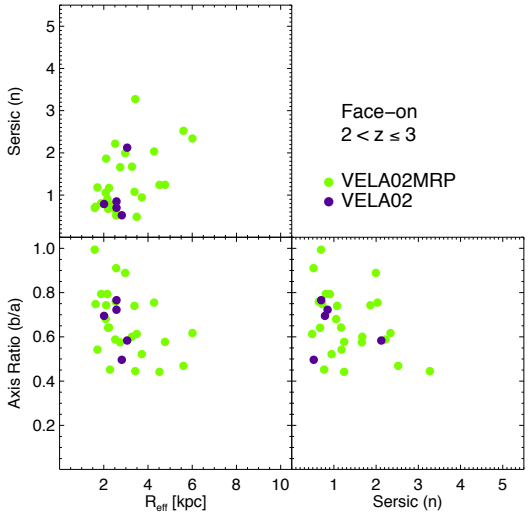
Face−on
2 < z ≤ 3
VELA02MRP
VELA02
Sersic (n)
Axis Ratio (b/a)
R_eff [kpc]
Sersic (n)

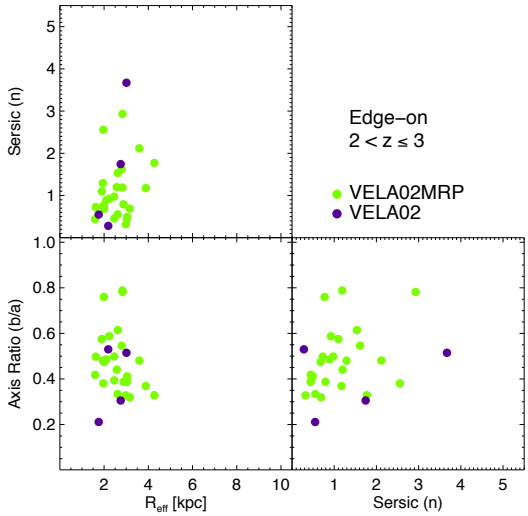
Edge−on
2 < z ≤ 3
VELA02MRP
VELA02
Sersic (n)
Axis Ratio (b/a)
R_eff [kpc]
Sersic (n)

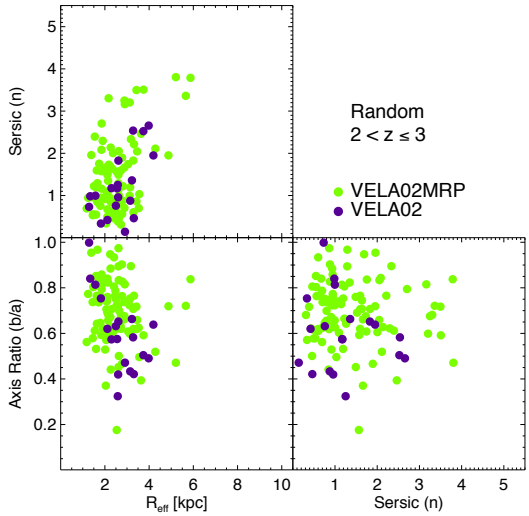
Random
2 < z ≤ 3
VELA02MRP
VELA02
Sersic (n)
Axis Ratio (b/a)
R_eff [kpc]
Sersic (n)

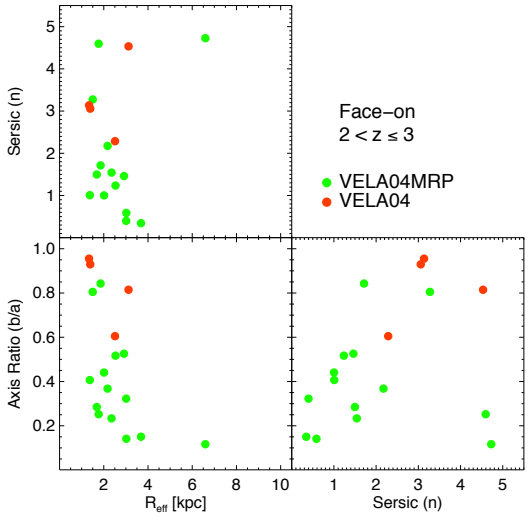
Face−on
2 < z ≤ 3
VELA04MRP
VELA04
Sersic (n)
Axis Ratio (b/a)
R_eff [kpc]
Sersic (n)

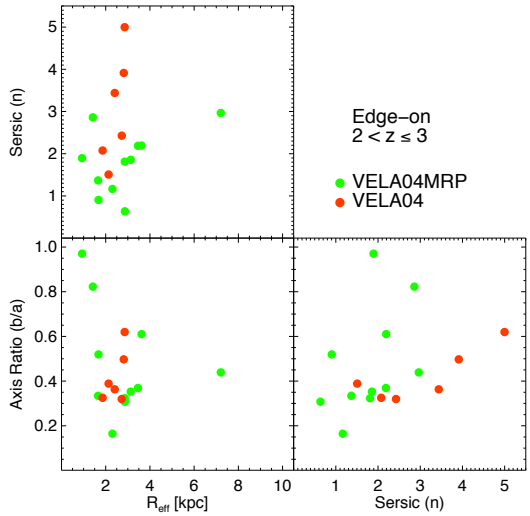
Edge−on
2 < z ≤ 3
VELA04MRP
VELA04
Sersic (n)
Axis Ratio (b/a)
R_eff [kpc]
Sersic (n)

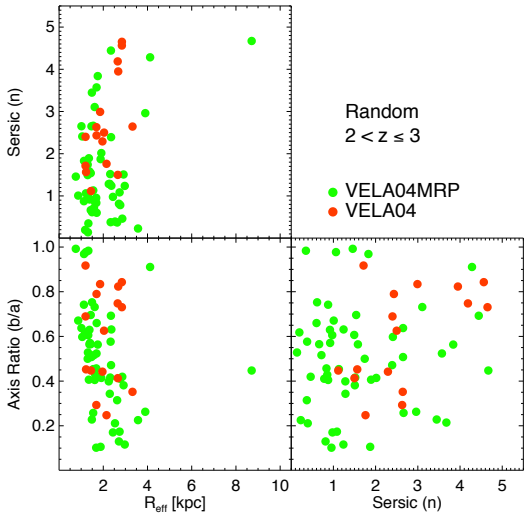
Random
2 < z ≤ 3
VELA04MRP
VELA04
Sersic (n)
Axis Ratio (b/a)
R_eff [kpc]
Sersic (n)

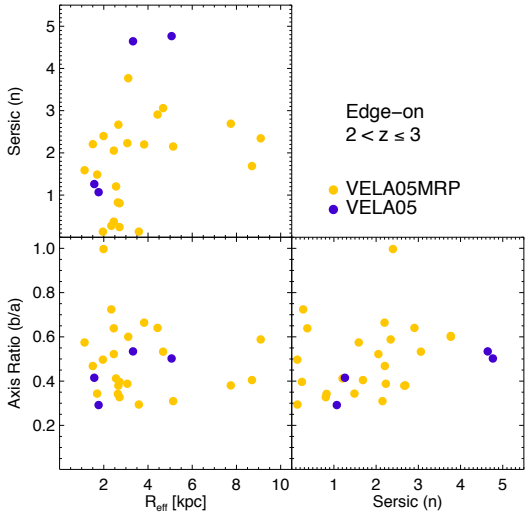
Edge−on
2 < z ≤ 3
VELA05MRP
VELA05
Sersic (n)
Axis Ratio (b/a)
R_eff [kpc]
Sersic (n)

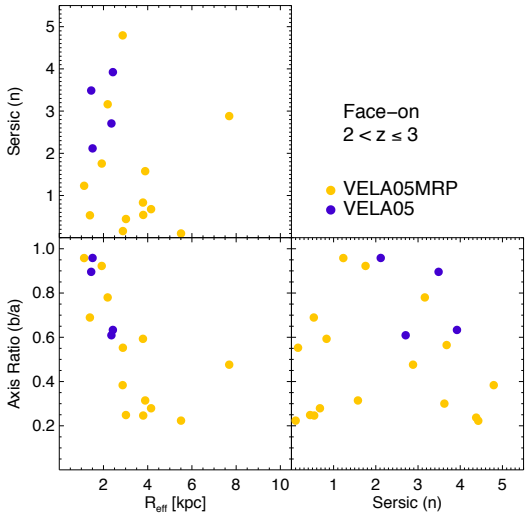
Face−on
2 < z ≤ 3
VELA05MRP
VELA05
Sersic (n)
Axis Ratio (b/a)
R_eff [kpc]
Sersic (n)

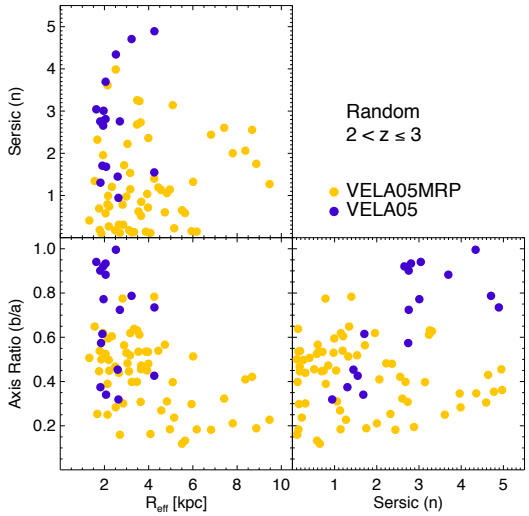
Random
2 < z ≤ 3
VELA05MRP
VELA05
Sersic (n)
Axis Ratio (b/a)
R_eff [kpc]
Sersic (n)

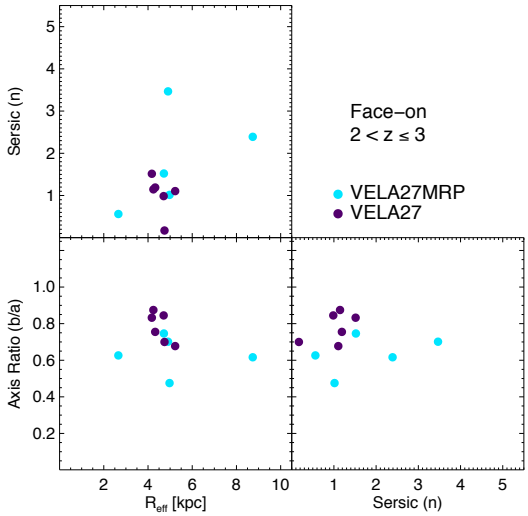
Face−on
2 < z ≤ 3
VELA27MRP
VELA27
Sersic (n)
Axis Ratio (b/a)
R_eff [kpc]
Sersic (n)

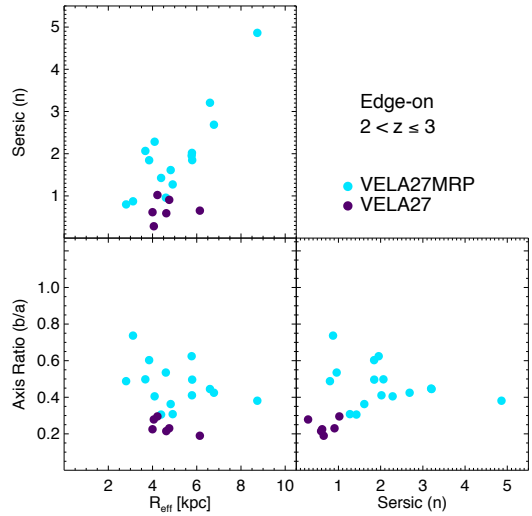
Edge-on
2 < z ≤ 3
VELA27MRP
VELA27
Sersic (n)
Axis Ratio (b/a)
R_eff [kpc]
Sersic (n)

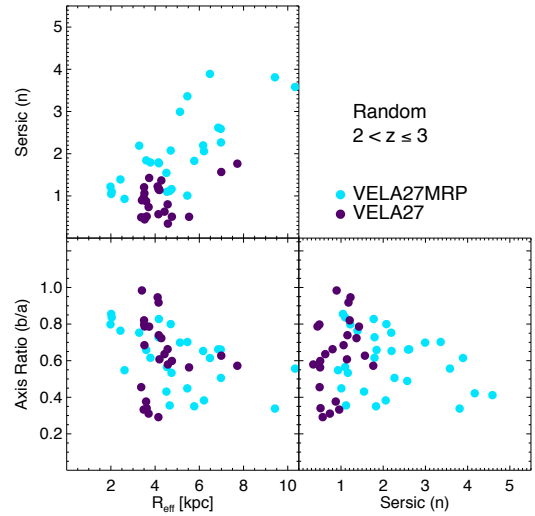
Random
2 < z ≤ 3
VELA27MRP
VELA27
Sersic (n)
Axis Ratio (b/a)
R_eff [kpc]
Sersic (n)

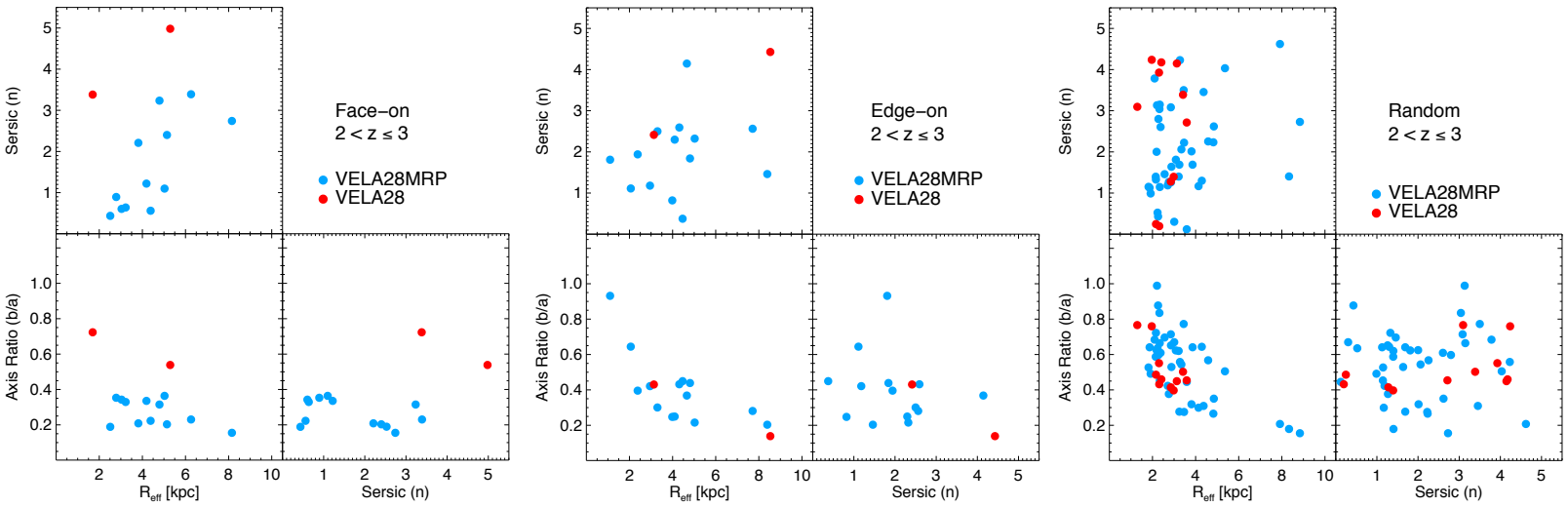

Figure 13: A three panel plot of axis ratio, R_{eff}, and Sérsic index of 5 simulations at $2 < z \leq 3$.

3.3 Image Inspection I

To verify the correctness of our inferred geometries from the analysis of GALFIT's best-fit parameters, we inspect some of the high resolution images and plot them as data points to see whether the axis ratios are reflected in these images, i.e., disks galaxies have low axis ratios. We select simulation 28 (VELA28 and VELA28MRP) for this investigation. The images used in this part of the analysis are composite images from 3 different waveband for edge-on and face-on angles. At $1 \leq z < 1.5$ all galaxies are both disks when viewed face-on with all axis ratios ≥ 0.7, where galaxies with RP have lower axis ratios than those without RP. From the edge-on analysis at the same redshifts, galaxies without RP have axis ratios ~ 2 and look very disk-like, whereas those with RP have axis ratios as high as ~ 0.5, and look less disk-like. This is in part of agreement with our conclusion from §3.1.1: the combination of face-on and edge-on analysis indicates that disk-like structure at low redshift do not reflect in the random viewing angles and towards higher redshifts there appears to have no hit of elongation. The issues are now then related to the random viewing angles and why we are unable to see clues of elongation toward higher z.

From §3.2.2 we found that at $1.5 \leq z < 2$, VELA28MRP, where at small radii the axis ratios and Sérsic indices have high values corresponding to spheroids, at larger radii ($R_{eff} >$ 4 kpc) both the axis ratios and Sérsic indices drop to lower values, implying that some of these galaxies are elongated. Judging from the images in Figure 14 and 15, we see that VELA28 at $1.5 \leq z < 2$ have high axis ratios (> 0.8) and look spheroidal face-on, while they look elongated when viewed edge-on. At the same redshifts, VELA28MRP looks more elongated with generally lower axis ratios; we expect that elongated objects to have axis ratios ~ 0.8 or greater when viewed face-on, but as one can see VELA28MRP is elongated *and* have a somewhat irregular appearance, where some even have small satellites. This becomes problematic for GALFIT as these small satellites prevent proper fitting, which can affect the Sérsic values and axis ratios as observed in the analysis at $z > 2$ in §3.2.3: VELA28MRP in random viewing angles exhibit the trend one expects to see if the the galaxy is elongated in the axis ratio vs. R_{eff} plot. At small radii these galaxies have higher axis ratios, corresponding to small spheroids. As the size increases the axis ratio decreases, corresponding to elongated objects. However, the wide range of Sérsic indices ($0 < n < 3$) at small radii is not a good indicator on whether these star-forming galaxies are spheroids, small disks, or some intermediate shape. It is clear that at $z > 2$, all galaxies in Figure 14 and 15 have minor mergers, which can cause more issues during the fit by GALFIT.

Investigation on random images showed that the 4 random angles are not truly ran-

dom. In the 4 random angles, which we presume to be truly random at each time step, were found to be the same for each camera. In other words, for example, camera 5 is one of the random viewing angles which turns out to have the same view for each galaxy at various redshifts, rather than random view at various redshifts. This implies that all the random plots analysis presented thus far should not be used as a reliable source for determining the shapes of the galaxies. The face-on and edge-on plots remain valid as far as the parameters' uncertainties concern, since all data points used for plotting have acceptable uncertainties. In the next section we investigate what caused GALFIT to yield large uncertainties for images that appear to be fine.

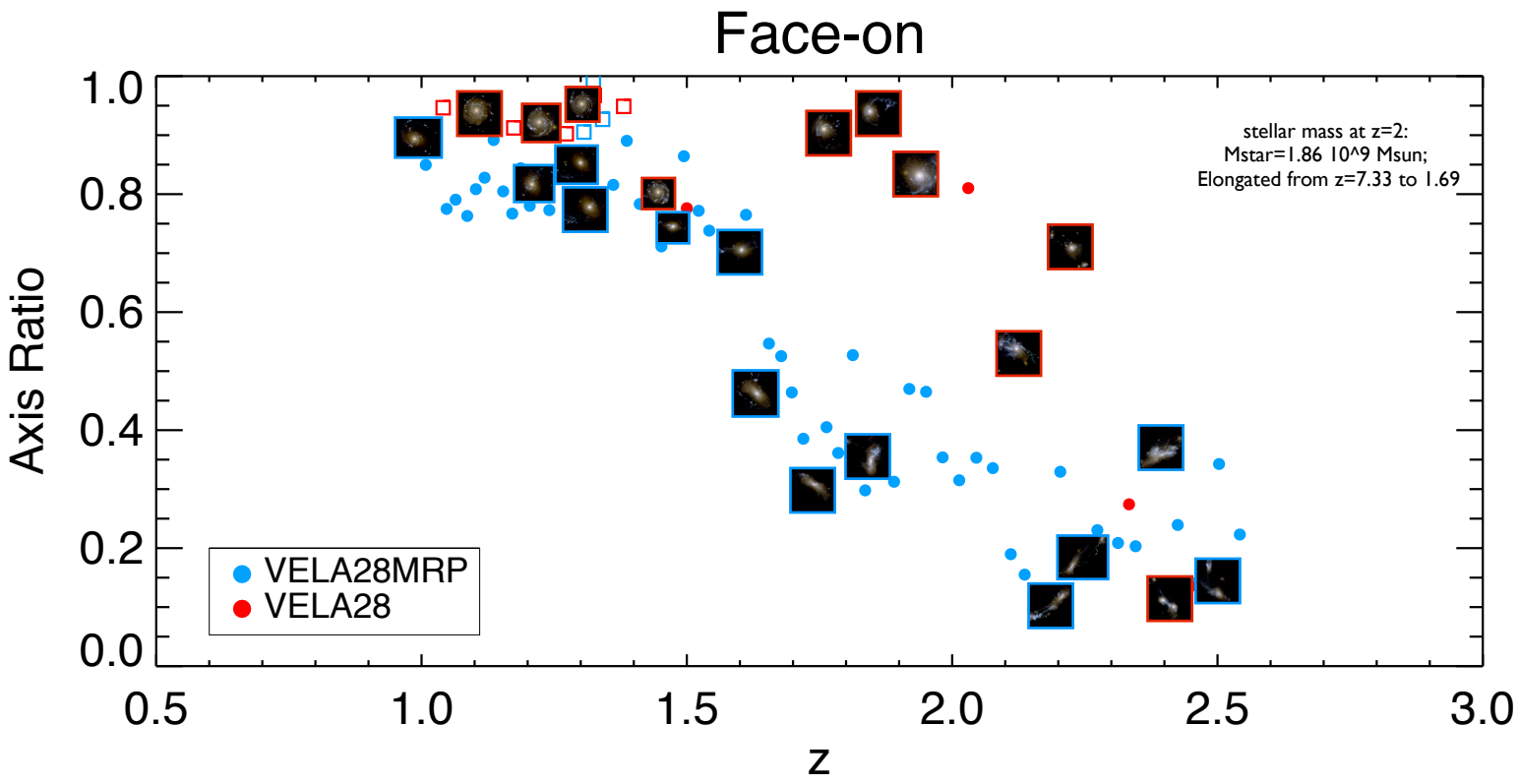

Figure 14: Axis ratio as a function of redshift as viewed face-on. Some data points are plotted using high resolution images where images of three different waveband were stacked together to create colour for the galaxy.

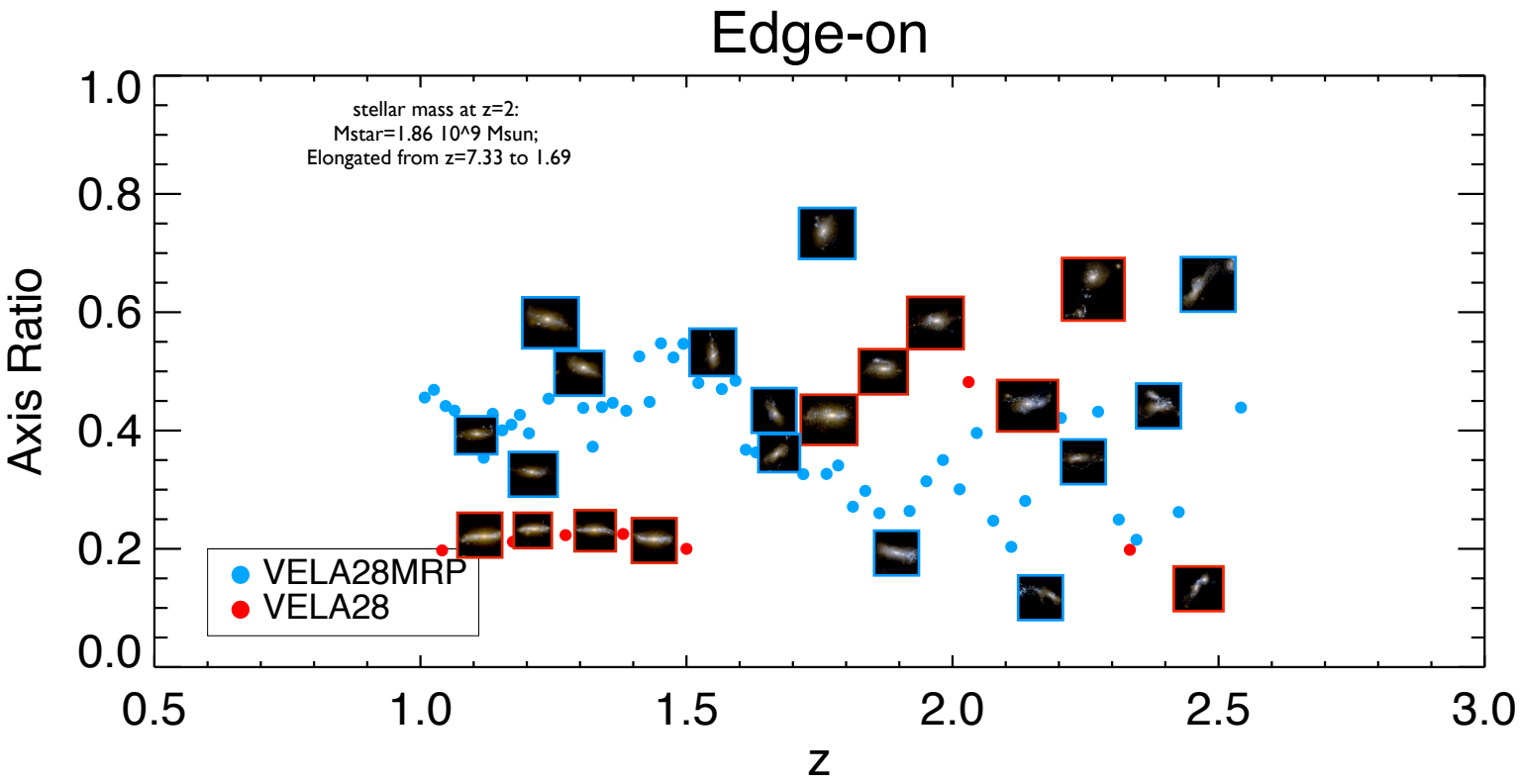

Figure 15: Axis ratio as a function of redshift as viewed edge-on. Some data points are plotted using high resolution images where images of three different waveband were stacked together to create colour for the galaxy.

3.4 Image Inspection II

We continue our image inspection using simulation 28 (VELA28 and VELA28MRP) with images in H band, one of the wavebands CANDELS uses for observing their galaxies, instead of high resolution images as we did in the previous section. As shown in Figures 16 to 21, where we use plots of axis ratio vs. R_{eff} (named as the Semi-major axis in the plots) with symbol coded Sérsic indices. Some of the data points have their corresponding H band images plotted next to it. We also inspect their corresponding residual images from GALFIT to check whether they were fitted properly, which are displayed next to the H band images. What we have learned from these plots:

- At $1 < z < 1.5$, all galaxies from VELA28 have uncertainties exceeded the acceptable range in the face-on viewing angle. This explains why there are no data points for VELA28 in the face-on plot in Figure 16 since they were excluded due to large uncertainties. They are however present in the edge-on view where GALFIT was able to fit their images properly. The residual maps (in grey) for VELA28 in Figure 16 are marked with red dotted boarder lines, with their Sérsic index, axis ratio, and R_{eff} listed next to the residual maps. They were exclude from the plot due to large uncertainties as reflected in extremely large/ small values for the parameter. The residual maps show the remaining component which for a proper fit should be subtracting them greatly. This is not the case and the best-fit parameters have values that are non-sensible.

- Most of the images for VELA28MRP at $1 < z < 1.5$ in face-on and edge-on views appear to be similar in size, yet their measured radii vary greatly. These images are surrounded with blue dotted border lines, and for very similar looking images their Sérsic indices also vary greatly, with some having zero values.

- Upon inspection, we find that GALFIT had trouble fitting due to the sky background value (skymode) being set as free parameter during the fit, rather than held fixed. All analysis for this work was done by allowing GALFIT to find the best-fit value for sky background (set as free parameter). We suspect that when it is held as a fixed parameter using a pre-calculated sky background (skymode) value associated to the image file, GALFIT can do a better job on fitting data images.

- At $1.5 < z < 2$ we see similar issues from studying the residual images, possibly caused by the sky background parameter as well as having small satellites (more than a one object in an image). Similarly, mergers at $z > 2$ will cause GALFIT to yield

non-sensible results by using a single-component fit. This is an issue for automated fitting for presumably each image contains only a single galaxy.

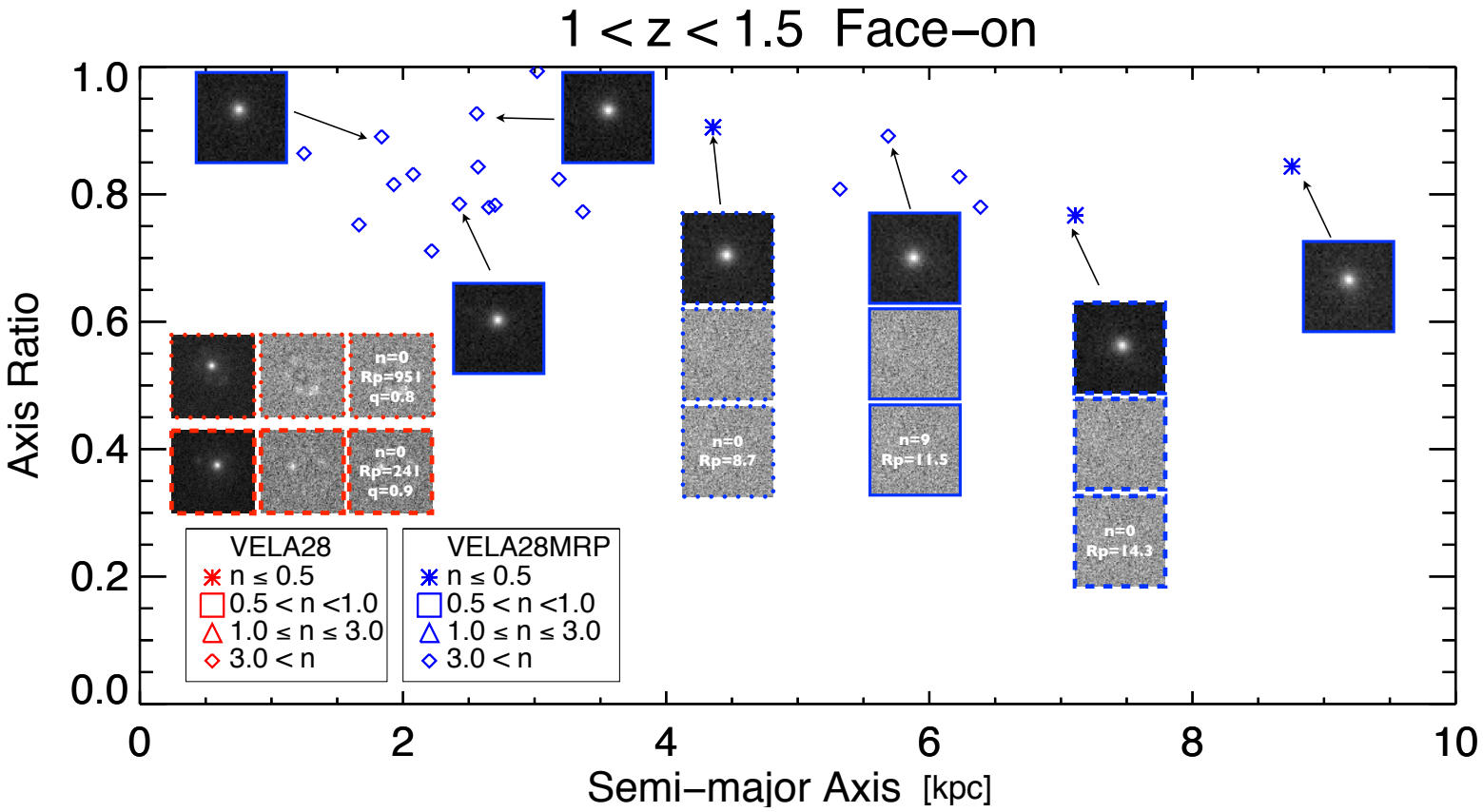

Figure 16: H band image inspection. Grey images are the residual maps of the data image from GALFIT.

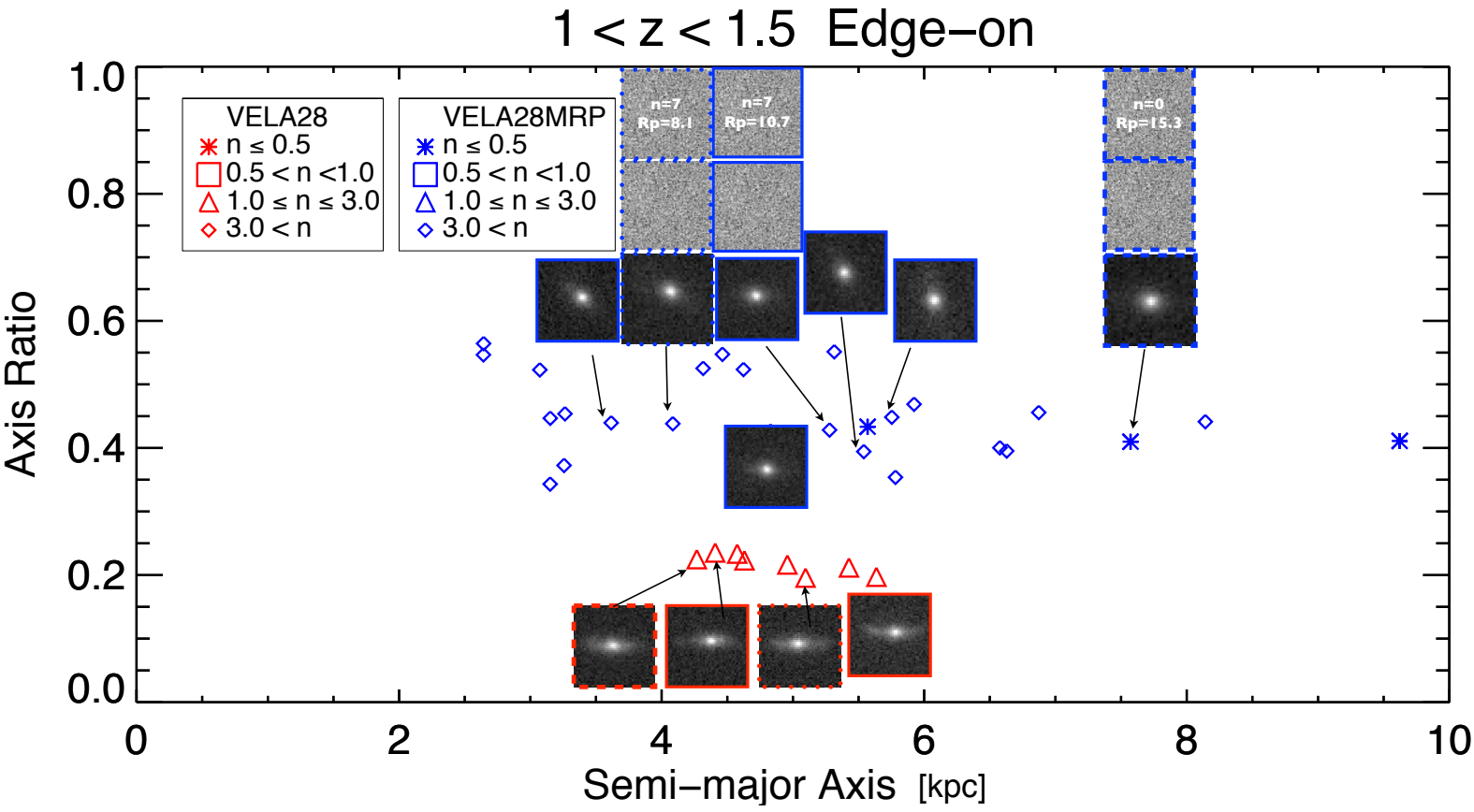

Figure 17: H band image inspection. Grey images are the residual maps of the data image from GALFIT.

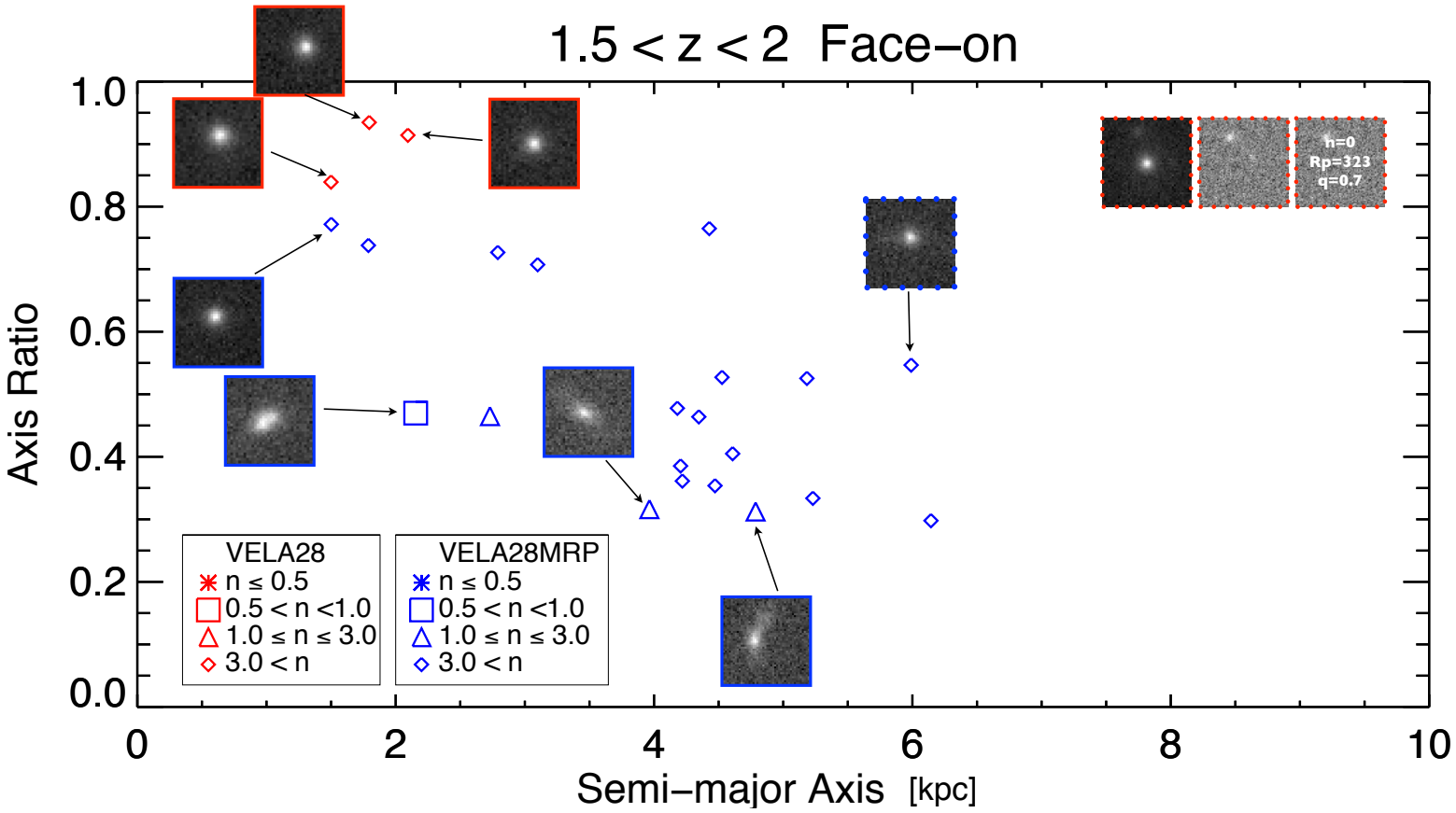

Figure 18: H band image inspection. Grey images are the residual maps of the data image from GALFIT.

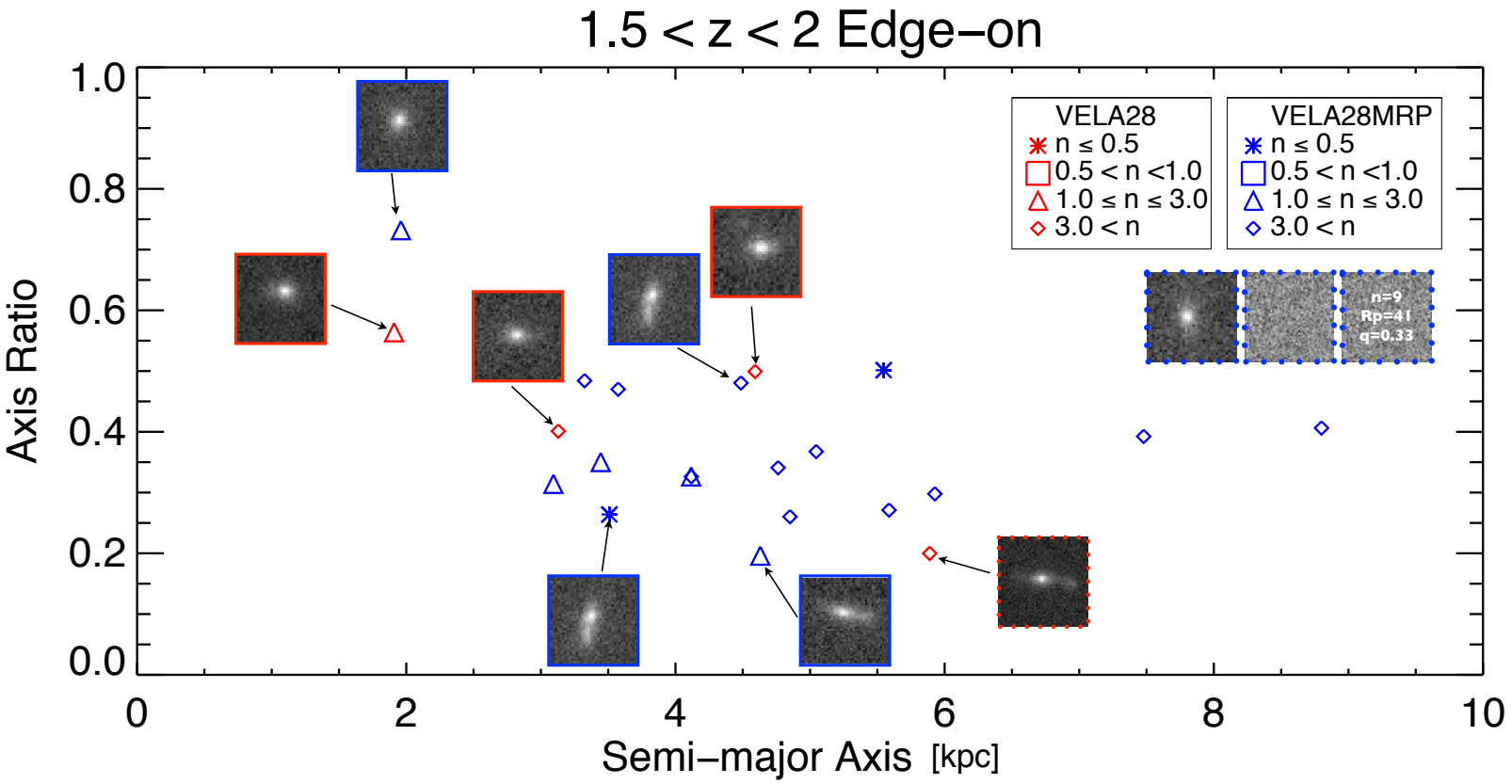

Figure 19: H band image inspection. Grey images are the residual maps of the data image from GALFIT.

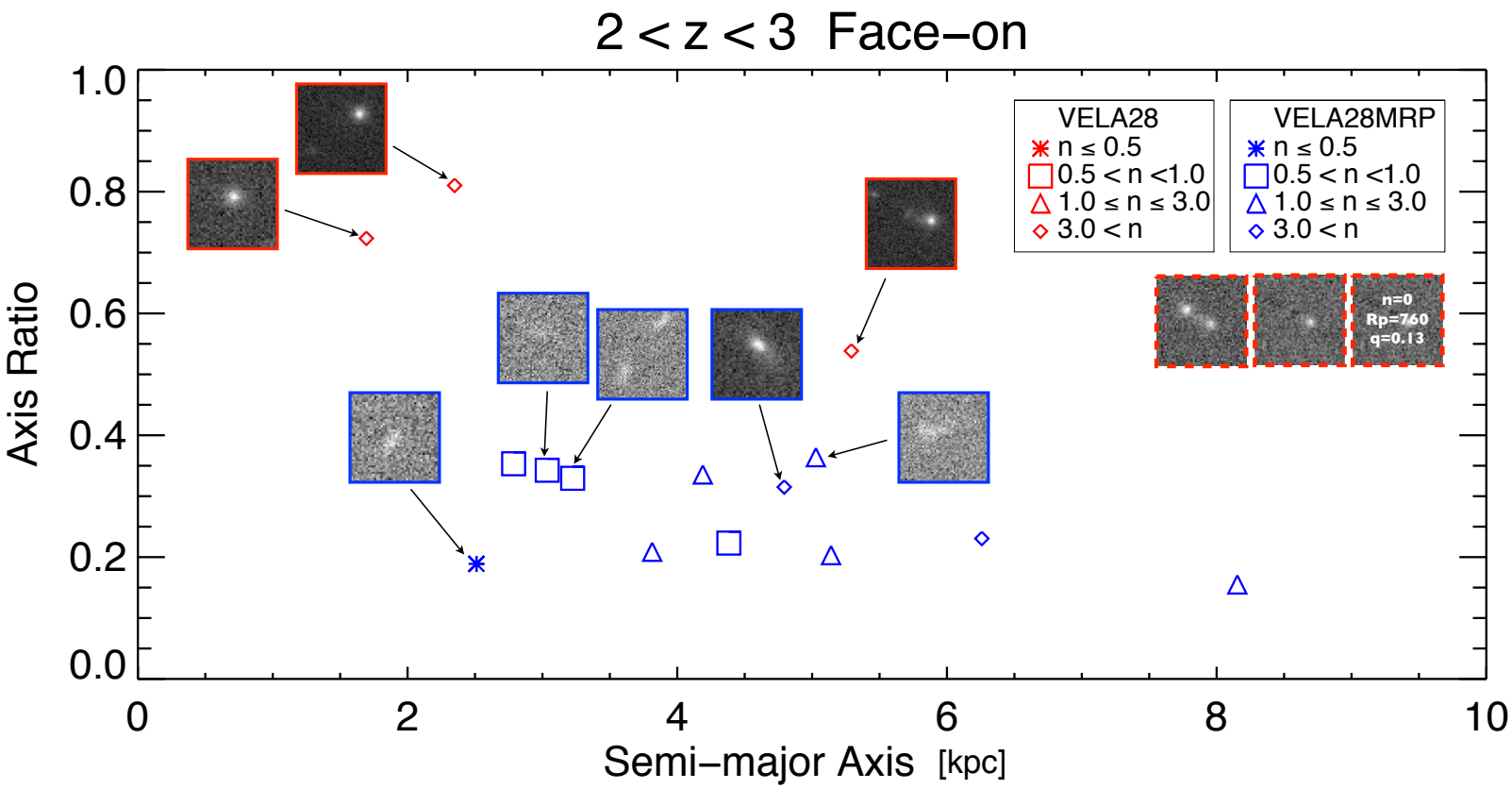

Figure 20: H band image inspection. Grey images are the residual maps of the data image from GALFIT.

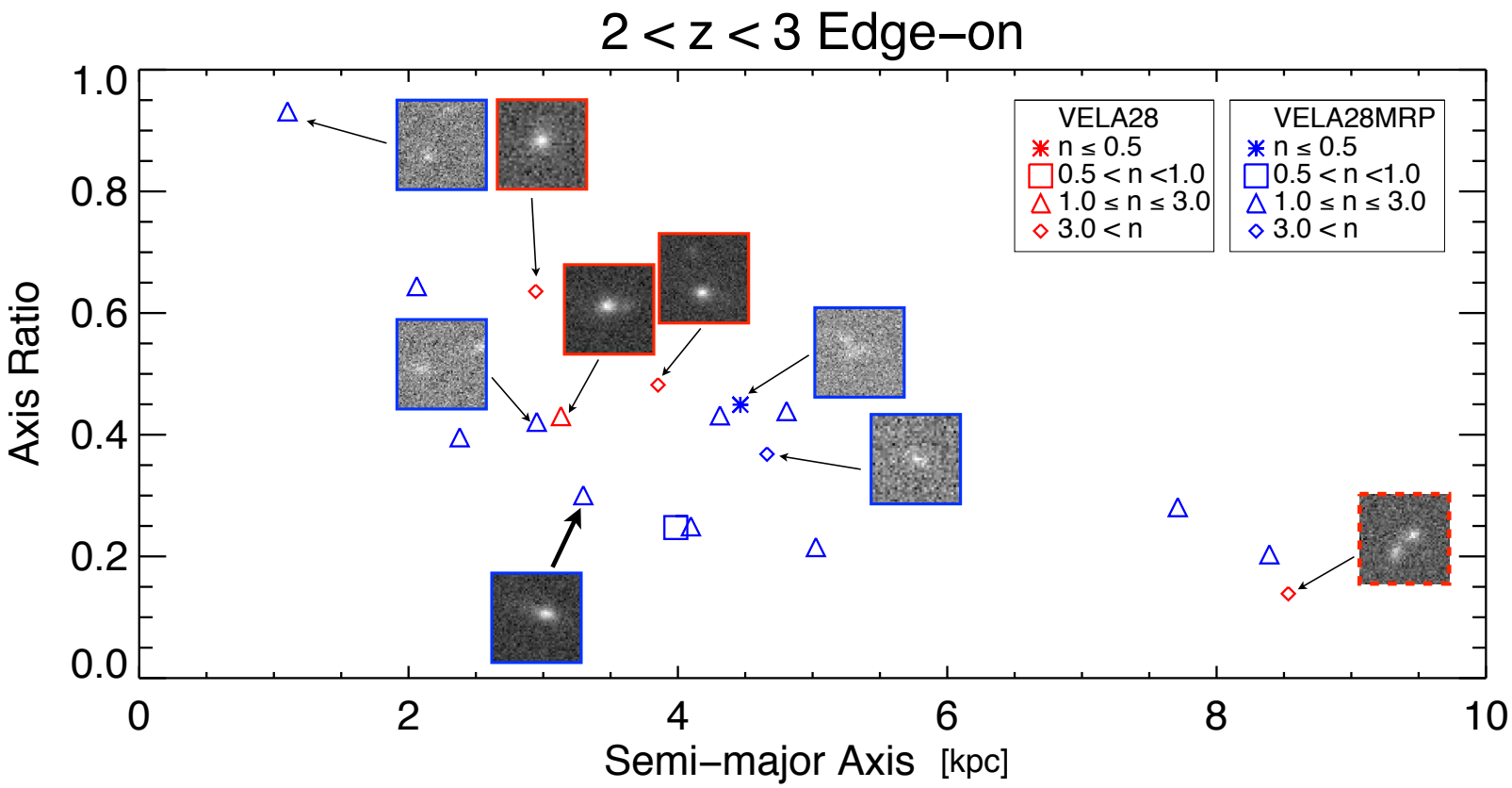

Figure 21: H band image inspection. Grey images are the residual maps of the data image from GALFIT.

4 Conclusions

Using observations of galaxies in CANDELS as comparisons, which indicated that a majority of star-forming galaxies with stellar masses less than about $10^{9.5} M_{\odot}$ are elongated at $1.5 < z < 2$, while for galaxies of similar stellar masses in the local Universe with the most common structures are disks and spheroids, we analyze star-forming galaxies from five pairs of cosmological simulation generated using the ART code. We create images of galaxies from the simulation in such a way that is comparable to HST observations. We obtain our images using the Sunrise code, which takes into account stellar evolution and the effects of dust. Their resolution is reduced and noise is added for proper comparison with CANDELS galaxy images, a process called CANDELization. There are two types of simulations: with and without RP feedback. Galaxies generated without RP feedback have SFR ~ 5 times higher than observation, resulting in overproduction of stars at early times with stellar mass systematically higher than galaxies generated with RP feedback. Although galaxies with RP feedback have SFR still ~ 2 times higher than observed galaxies from CANDELS, we find that, by analyzing the surface brightness distribution of our simulated galaxies via structural parameters R_{eff}, Sérsic index n, and projected axis ratio provided by GALFIT as best-fit parameters, four out of five simulations (02, 05, 27, 28) with RP produce galaxies that are similar to those observed by CANDELS. Each of the four simulations have stellar masses comparable to those of CANDELS, and we find that:

- At $z \sim 2$ VELA02MRP are elongated and have stellar mass $10^{9.4} M_{\odot}$.
- At $1.5 < z < 2$ VELA05MRP are elongated and have stellar mass $10^{9.3} - 10^{9.6} M_{\odot}$.
- At $1.5 < z < 2$ VELA27MRP are elongated and have stellar mass $10^{10} - 10^{10.3} M_{\odot}$.
- Galaxies from VELA28MRP are likely to be elongated at $z \sim 1.5$ from the analysis on structural parameters, and from inspecting their images in both high-resolution and H band we find that they look elongated at $1.5 < z < 2$. The stellar masses are $10^{9.5} M_{\odot}$ at $z \sim 2$ and $10^{9.8} M_{\odot}$ at $z \sim 1$.

In most cases, galaxies are disks at $z < 1.5$ and beyond $z \sim 2.5$ there exists a mixture of irregular shapes and minor mergers. These findings are similar to the result from the analysis of star-forming galaxies from CANDELS, where the shapes of the galaxies were determined based on projected axis ratios of a triaxial ellipsoid population. These galaxies are elongated at $1.5 < z < 2$ for stellar masses $10^{9.5} - 10^{10} M_{\odot}$ and at $1 < z < 2.5$ for stellar masses $10^{9} - 10^{9.5} M_{\odot}$, with disk-like structures at $z < 1.5$. From our simulation, in every

case, galaxies without RP evolve differently than galaxies with RP as expected from the known morphological dependence on SFR and stellar mass; results of galaxies without RP are less conclusive due to too few data points. The shapes of our simulated galaxies are deduced from studying their best-fit parameters separated in face-on, edge-on, and random viewing angles. We find that in all cases results from random views do not correlate well with the infer shapes from face-on and edge-on analysis and vice versa. We find that this is due to random angles not being truly random. Upon inspecting images of galaxies from simulation 28, we determine that GALFIT was unable to successfully fit certain images due to, in some cases, images contain multiple objects, and in other cases where the best-fit parameters having large uncertainties correspond to a poorly defined sky background parameter in GALFIT. Because all simulations with RP used for this study have stellar masses in the lower range, we suspect that for those that were not found to have shapes similar to CANDELS galaxies would yield a different conclusion if GALFIT is able to do a better job at fitting these images. We will continue our analysis on more simulations and compare the morphology between galaxies generated with different levels of RP feedback as well as reanalyzing simulations used in this study with the proper parameters provided to GALFIT.

5 Bibliography

References

Behroozi, P. S., Wechsler, R. H., and Conroy, C. 2013. The Average Star Formation Histories of Galaxies in Dark Matter Halos from z = 0-8. , **770**(June), 57.

Ceverino, Daniel, Klypin, Anatoly, Klimek, Elizabeth S., Trujillo-Gomez, Sebastian, Churchill, Christopher W., Primack, Joel, and Dekel, Avishai. 2014. Radiative feedback and the low efficiency of galaxy formation in low-mass haloes at high redshift. *Monthly Notices of the Royal Astronomical Society*, **442**(2), 1545–1559.

Finkelstein, S. L., Papovich, C., Dickinson, M., Song, M., Tilvi, V., Koekemoer, A. M., Finkelstein, K. D., Mobasher, B., Ferguson, H. C., Giavalisco, M., Reddy, N., Ashby, M. L. N., Dekel, A., Fazio, G. G., Fontana, A., Grogin, N. A., Huang, J.-S., Kocevski, D., Rafelski, M., Weiner, B. J., and Willner, S. P. 2013. A galaxy rapidly forming stars 700 million years after the Big Bang at redshift 7.51. , **502**(Oct.), 524–527.

Guo, Y., Ferguson, H. C., Bell, E. F., Koo, D. C., Conselice, C. J., Giavalisco, M., Kassin, S., Lu, Y., Lucas, R., Mandelker, N., McIntosh, D. M., Primack, J. R., Ravindranath, S., Barro, G., Ceverino, D., Dekel, A., Faber, S. M., Fang, J. J., Koekemoer, A. M., Noeske, K., Rafelski, M., and Straughn, A. 2015. Clumpy Galaxies in CANDELS. I. The Definition of UV Clumps and the Fraction of Clumpy Galaxies at $0.5 < z < 3$. , **800**(Feb.), 39.

Jonsson, P. 2006. SUNRISE: polychromatic dust radiative transfer in arbitrary geometries. , **372**(Oct.), 2–20.

Loeb, Abraham. 2010. *How Did the First Stars and Galaxies Form?* Princeton University Press.

Moody, C. E., Guo, Y., Mandelker, N., Ceverino, D., Mozena, M., Koo, D. C., Dekel, A., and Primack, J. 2014. Star formation and clumps in cosmological galaxy simulations with radiation pressure feedback. , **444**(Oct.), 1389–1399.

Neistein, E., van den Bosch, F. C., and Dekel, A. 2006. Natural downsizing in hierarchical galaxy formation. , **372**(Oct.), 933–948.

O'Leary, E. M., and Kartaltepe, J. S. 2013 (Jan.). Galaxy Merger Identification in the

CANDELS GOODS-South Field. Page 147.33 of: *American Astronomical Society Meeting Abstracts #221*. American Astronomical Society Meeting Abstracts, vol. 221.

Peng, Chien Y. *SIGMA (σ) IMAGE AND CHI^2 (χ^2) FAQ*. http://users.obs.carnegiescience.edu/peng/work/galfit/CHI2.html.

Peng, Chien Y. *Top 10 Rules of Thumb for Galaxy Fitting*. http://users.obs.carnegiescience.edu/peng/work/galfit/TFAQ.html.

Peng, Chien Y. 2007 (7). *GALFIT USER'S MANUAL*. http://users.obs.carnegiescience.edu/peng/work/galfit/README.pdf.

Snyder, G. F., Lotz, J., Moody, C., Peth, M., Freeman, P., Ceverino, D., Primack, J., and Dekel, A. 2014. Diverse Structural Evolution at z $>$ 1 in Cosmologically Simulated Galaxies. *ArXiv e-prints*, Sept.

van der Wel, A., Chang, Y.-Y., Bell, E. F., Holden, B. P., Ferguson, H. C., Giavalisco, M., Rix, H.-W., Skelton, R., Whitaker, K., Momcheva, I., Brammer, G., Kassin, S. A., Martig, M., Dekel, A., Ceverino, D., Koo, D. C., Mozena, M., van Dokkum, P. G., Franx, M., Faber, S. M., and Primack, J. 2014. Geometry of Star-forming Galaxies from SDSS, 3D-HST, and CANDELS. , **792**(Sept.), L6.

Wuyts, S., Förster Schreiber, N. M., van der Wel, A., Magnelli, B., Guo, Y., Genzel, R., Lutz, D., Aussel, H., Barro, G., Berta, S., Cava, A., Graciá-Carpio, J., Hathi, N. P., Huang, K.-H., Kocevski, D. D., Koekemoer, A. M., Lee, K.-S., Le Floc'h, E., McGrath, E. J., Nordon, R., Popesso, P., Pozzi, F., Riguccini, L., Rodighiero, G., Saintonge, A., and Tacconi, L. 2011. Galaxy Structure and Mode of Star Formation in the SFR-Mass Plane from z $\sim$ 2.5 to z $\sim$ 0.1. , **742**(Dec.), 96.